

A Pre-Training and Adaptive Fine-Tuning Framework for Graph Anomaly Detection

Yunhui Liu*
 lyhcloudy1225@gmail.com
 Nanjing University
 Nanjing, China

Fugee Tsung
 season@ust.hk
 HKUST(GZ), HKUST
 Guangzhou/Hong Kong SAR, China

Jiashun Cheng*
 jchengak@connect.ust.hk
 HKUST
 Hong Kong SAR, China

Hongzhi Yin
 h.yin1@uq.edu.au
 The University of Queensland
 Brisbane, Australia

Jia Li
 jialee@ust.hk
 HKUST(GZ), HKUST
 Guangzhou/Hong Kong SAR, China

Tieke He
 hetieke@gmail.com
 Nanjing University
 Nanjing, China

Abstract

Graph anomaly detection (GAD) has garnered increasing attention in recent years, yet it remains challenging due to the scarcity of abnormal nodes and the high cost of label annotations. Graph pre-training, the two-stage learning paradigm, has emerged as an effective approach for label-efficient learning, largely benefiting from expressive neighborhood aggregation under the assumption of strong homophily. However, in GAD, anomalies typically exhibit high local heterophily, while normal nodes retain strong homophily, resulting in a complex homophily-heterophily mixture. To understand the impact of this mixed pattern on graph pre-training, we analyze it through the lens of spectral filtering and reveal that relying solely on a global low-pass filter is insufficient for GAD. We further provide a theoretical justification for the necessity of selectively applying appropriate filters to individual nodes. Building upon this insight, we propose PAF, a Pre-Training and Adaptive Fine-tuning framework specifically designed for GAD. In particular, we introduce joint training with low- and high-pass filters in the pre-training phase to capture the full spectrum of frequency information in node features. During fine-tuning, we devise a gated fusion network that adaptively combines node representations generated by both filters. Extensive experiments across ten benchmark datasets consistently demonstrate the effectiveness of PAF. The code is available at <https://anonymous.4open.science/r/PAF-163E>.

CCS Concepts

• Computing methodologies → Machine learning

Keywords

Graph Anomaly Detection, Graph Pre-Training, Graph Neural Networks

*Equal Contribution

Permission to make digital or hard copies of all or part of this work for personal or classroom use is granted without fee provided that copies are not made or distributed for profit or commercial advantage and that copies bear this notice and the full citation on the first page. Copyrights for components of this work owned by others than the author(s) must be honored. Abstracting with credit is permitted. To copy otherwise, or republish, to post on servers or to redistribute to lists, requires prior specific permission and/or a fee. Request permissions from permissions@acm.org.

Conference acronym 'XX, June 03–05, 2018, Woodstock, NY

© 2018 Copyright held by the owner/author(s). Publication rights licensed to ACM. ACM ISBN 978-1-4503-XXXX-X/18/06
<https://doi.org/XXXXXXX.XXXXXXX>

ACM Reference Format:

Yunhui Liu, Jiashun Cheng, Jia Li, Fugee Tsung, Hongzhi Yin, and Tieke He. 2018. A Pre-Training and Adaptive Fine-Tuning Framework for Graph Anomaly Detection. In *Proceedings of Make sure to enter the correct conference title from your rights confirmation email (Conference acronym 'XX)*. ACM, New York, NY, USA, 20 pages. <https://doi.org/XXXXXXX.XXXXXXX>

1 Introduction

Graph anomaly detection (GAD) aims to identify abnormal instances, such as nodes, that exhibit behavior deviating from the majority [39]. These anomalies are much less common than regular nodes, yet their detection is crucial for applications with significant social impact, such as identifying fraud in financial transaction graphs [59], detecting misinformation and fake news in social networks [52], and identifying spam reviews in user-rating-product graphs [9].

Graph neural networks (GNNs) have recently emerged as the leading approach for GAD due to their superior performance. Several studies [5, 10, 43] formulate GAD as a supervised binary classification problem, designing specialized GNN architectures to achieve state-of-the-art results. However, these methods rely heavily on a large number of labeled abnormal nodes, necessitating costly annotations of anomalies [32]. Concurrently, another line of research [24, 28, 38] treats GAD as a fully unsupervised problem, assuming no labeled information is available. While these methods eliminate the need for annotations, their inability to leverage even limited supervision leads to a significant performance gap compared to supervised approaches [40]. In real-world GAD scenarios, where labeled anomalies are scarce, developing more effective data mining strategies to maximize the utility of available information remains a critical challenge.

Graph pre-training has recently emerged as a promising solution to this challenge [6, 19, 50]. This learning paradigm is typically structured into two stages: pre-training and fine-tuning. In the pre-training phase, the encoder is optimized to capture universal knowledge, such as the general structural and relational patterns, from unlabeled data through self-supervised objectives. Two well-established self-supervised paradigms, contrastive learning [46, 57] and predictive learning [16, 44], have been widely adopted. During fine-tuning, a simple classifier is trained with supervision to adapt the pre-trained representations to specific downstream GAD tasks. Notably, a recent study [6] has demonstrated that this

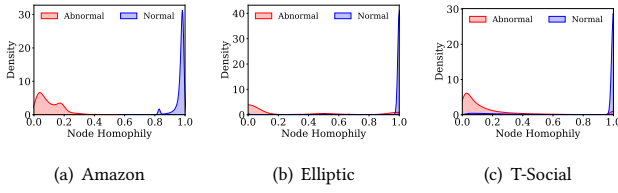


Figure 1: Distribution of node homophily on Amazon, Elliptic, and T-Social. GAD graphs display a mixed homophily-heterophily pattern: 1) Different nodes exhibit varying degrees of homophily/heterophily, and 2) Abnormal nodes tend to show higher heterophily than normal nodes. Visualizations for other datasets are shown in Figure 7.

two-stage paradigm can achieve performance on par with state-of-the-art supervised models for GAD with limited supervision. This finding highlights its potential to reduce dependence on costly label annotations while offering broader applicability across various real-world GAD scenarios.

Nonetheless, directly adapting graph pre-training to GAD inherently leads to sub-optimal performance. Most existing pre-training methods [16, 29, 44, 46, 55] implicitly assume strong homophily, where connected nodes tend to share the same label. Consequently, these methods typically utilize GNNs concentrating on neighborhood aggregation (e.g., GCN [21]) for universal knowledge acquisition in the pre-training phase. However, this homophily-driven design is inherently ill-equipped for heterophilic graphs, where nodes frequently connect to others with different labels – a characteristic prevalent in GAD settings. For example, fraudulent entities often exhibit camouflaged behaviors to obscure their connections with other fraudsters, resulting in a high degree of heterophily in fraud detection graphs [9]. In addition, [30] theoretically establishes that the heterophily of abnormal nodes is significantly higher than normal nodes, due to the class imbalance inherent in GAD. Empirically, as presented in Figures 1 and 7, a mixed homophily-heterophily pattern is consistently observed in the distributions of node homophily across various GAD benchmark datasets. Thus, a crucial question arises: *Can we design a pre-training framework tailored for the mixed homophily-heterophily pattern in GAD?*

Present Work. In this paper, we first systematically investigate the impact of the mixed homophily-heterophily pattern on graph pre-training through the lens of spectral analysis. Our analysis reveals the limitations of relying solely on low-pass filters and highlights the potential benefits of incorporating high-pass filters. We further provide a theoretical justification for the necessity of selectively applying spectral filters at the node level to handle varying homophily-heterophily patterns. Building on these insights, we propose PAF, a Pre-Training and Adaptive Fine-tuning framework tailored for GAD. PAF first pre-trains separate low- and high-pass filters to capture distinct spectral features embedded within node attributes across different frequencies. During fine-tuning, it employs a gated fusion network to adaptively generate the most informative node representations, optimizing them for GAD tasks. Moreover, the modular nature of PAF enables its seamless integration as a plug-and-play framework compatible with various

graph pre-training methods. We conduct extensive experiments on 10 benchmark datasets, comparing PAF against 17 state-of-the-art GAD and pre-training methods across different levels of supervision. Experimental results show that PAF consistently outperforms existing methods, showcasing both superior performance and strong generalizability as an enhancement to pre-training techniques.

2 Preliminaries

Notations. In a general scenario, we are given an attributed graph $\mathcal{G} = (\mathcal{V}, \mathcal{E}, \mathcal{X})$, where $\mathcal{V} = \{v_1, \dots, v_n\}$ is the set of n nodes, $\mathcal{E} = \{e_{ij}\}$ is the set of edges, and $e_{ij} = (v_i, v_j)$ represents an edge between nodes v_i and v_j . We define \mathbf{A} as the corresponding adjacency matrix and \mathbf{D} as the diagonal degree matrix with $D_{ii} = d_i = \sum_j A_{ij}$. The neighbor set \mathcal{N}_i of each node v_i is given by $\mathcal{N}_i = \{v_j : e_{ij} \in \mathcal{E}\}$. For each node v_i , it has a d -dimensional feature vector $\mathbf{x}_i \in \mathbb{R}^d$, and collectively the features of all nodes are denoted as $\mathcal{X} = (\mathbf{x}_1, \dots, \mathbf{x}_n)^\top \in \mathbb{R}^{n \times d}$.

2.1 Graph Anomaly Detection

Typically, graph anomaly detection is viewed as a binary classification problem where anomalies are regarded as positive with label 1 while normal nodes are negative with label 0. Given $\mathcal{V}^L = \mathcal{V}_a \cup \mathcal{V}_n$, where \mathcal{V}_a consists of labeled abnormal nodes and \mathcal{V}_n comprises labeled normal nodes, along with their corresponding labels \mathbf{y}^L , the goal is to identify the anomalous status $\hat{\mathbf{y}}^U$ for the unlabeled nodes $\mathcal{V}^U = \mathcal{V} \setminus \mathcal{V}^L$. Usually, obtaining authentic labels is often costly, we assume that label information is only available for a small subset of nodes (i.e., $|\mathcal{V}^L| \ll |\mathcal{V}|$). Furthermore, there are usually significantly fewer abnormal nodes than normal nodes (i.e., $|\mathcal{V}_a| \ll |\mathcal{V}_n|$).

2.2 Graph Spectral Filtering

Given the adjacency matrix \mathbf{A} , the graph Laplacian matrix is defined as $\mathbf{L} = \mathbf{D} - \mathbf{A}$, which is symmetric and positive semi-definite. Its eigendecomposition is given by $\mathbf{L} = \mathbf{U}\Lambda\mathbf{U}^\top$, where the columns of $\mathbf{U} \in \mathbb{R}^{n \times n}$ are orthonormal eigenvectors (graph Fourier basis), and $\Lambda = \text{diag}(\lambda_1, \lambda_2, \dots, \lambda_n)$ contains the eigenvalues (frequencies), arranged such that $0 = \lambda_1 \leq \lambda_2 \leq \dots \leq \lambda_n$. Given the graph features \mathcal{X} and a filter function $g(\cdot)$, the corresponding filtered features is thus defined as $\hat{\mathcal{X}} = \mathbf{U}g(\Lambda)\mathbf{U}^\top \mathcal{X}$.

In addition to \mathbf{A} and \mathbf{L} , some variants are also commonly used, e.g., symmetric normalized $\mathbf{A}_{sym} = \mathbf{D}^{-1/2}\mathbf{A}\mathbf{D}^{-1/2}$ and $\mathbf{L}_{sym} = \mathbf{I} - \mathbf{A}_{sym}$; random walk normalized $\mathbf{A}_{rw} = \mathbf{D}^{-1}\mathbf{A}$ and $\mathbf{L}_{rw} = \mathbf{I} - \mathbf{D}^{-1}\mathbf{A}$. Typically, \mathbf{A}_{sym} and \mathbf{A}_{rw} act as low-pass filters with $g(\lambda) = 1 - \lambda$, while $-\mathbf{A}_{sym}$, $-\mathbf{A}_{rw}$, \mathbf{L}_{sym} , and \mathbf{L}_{rw} serve as high-pass filters, with $g(\lambda) = \lambda - 1$ and $g(\lambda) = \lambda$, respectively. In practice, a self-loop is often added to each node in the graph (i.e., $\mathbf{A} = \mathbf{A} + \mathbf{I}$) to alleviate numerical instabilities and improve performance [21].

2.3 Homophily and Heterophily

Homophily refers to the tendency of edges to connect nodes with the same label, whereas heterophily describes the opposite phenomenon. There are three commonly used homophily metrics: edge homophily, node homophily, and class homophily.

Edge homophily [56] is defined as the fraction of intra-class edges in the graph:

$$h = \frac{|\{e_{ij} \in \mathcal{E} : y_i = y_j\}|}{|\mathcal{E}|}. \quad (1)$$

Node homophily [36] measures the fraction of a node's neighbors that share the same label:

$$h_i = \frac{|\{j \in \mathcal{N}_i : y_i = y_j\}|}{|\mathcal{N}_i|}. \quad (2)$$

Class homophily [31] here computes the average node homophily for anomalous and normal nodes, respectively:

$$h^a = \frac{\sum_{y_i=1} h_i}{\sum_{y_i=1} 1}, \quad h^n = \frac{\sum_{y_i=0} h_i}{\sum_{y_i=0} 1}. \quad (3)$$

Note that all these metrics lie within the range $[0, 1]$. Graphs or nodes with a higher proportion of intra-class edges exhibit greater homophily. In Table 3, we provide the values of h , h^a , and h^n for each dataset. As presented, h^a is much smaller than h^n , indicating that abnormal nodes exhibit significantly higher heterophily compared to normal ones.

3 Motivation

In this section, we first examine the influence of mixed homophily-heterophily patterns on graph pre-training, highlighting the limitations of employing a single global low-pass filter. Building upon this, we further justify the necessity of applying appropriate filters to individual nodes to enhance learning capacity in GAD.

3.1 Analysis from Spectral View

Without loss of generality, we suppose the dimension of input features $d = 1$ with $\mathbf{X} \in \mathbb{R}^n$ in this section. Let $\mathbf{y}_i \in \{0, 1\}$ with $\mathbf{y}_i = 1$ representing abnormal nodes, and define $\Delta\mathbf{y} \in \mathbb{R}^n$ as the difference in node labels. Here, we consider graph Laplacian matrix $\mathbf{L} = \mathbf{D} - \mathbf{A}$.

We investigate the impact of the homophily-heterophily mixture via the lens of spectral filtering. From the spectral view, graph pre-training for GAD can decoupled into two stages: (1) Pre-training phase generates $\hat{\mathbf{X}} = \mathbf{U}g(\Lambda)\mathbf{U}^\top \mathbf{X} \in \mathbb{R}^n$, where $g(\cdot)$ is typically a low-pass filter; (2) Fine-tuning phase produces $\hat{\mathbf{y}} = \sigma(\text{MLP}(\hat{\mathbf{X}})) \in \mathbb{R}^n$, where $\sigma(\cdot)$ is the activation function and $\hat{\mathbf{X}}$ is frozen.

Essentially, the desirable graph filtering in pre-training should produce distinguishable node representations $\hat{\mathbf{X}}$ associated with $\Delta\mathbf{y}$ to identify abnormal nodes. For an in-depth probing, let $\boldsymbol{\alpha} = \mathbf{U}^\top \Delta\mathbf{y} = (\alpha_1, \dots, \alpha_n) \in \mathbb{R}^n$ and $\boldsymbol{\beta} = \mathbf{U}^\top \mathbf{X} = (\beta_1, \dots, \beta_n) \in \mathbb{R}^n$ be the spectra of $\Delta\mathbf{y}$ and \mathbf{X} , we first obtain the following results:

PROPOSITION 1. *For a binary graph anomaly detection problem, let α_i^2 be the spectral energy of $\Delta\mathbf{y}$ at frequency λ_i , its total spectral energy is constant with $\sum_{i=1}^n \alpha_i^2 = n$ and concentrates more on high frequencies as the heterophily of abnormal nodes increases.*

The detailed proof is provided in Appendix B.1. Proposition 1 implies that more emphasis on capturing the information of $\Delta\mathbf{y}$ at higher frequencies may be required when faced with a higher level of heterophily as in the tasks of anomaly detection. Meanwhile, inspired by [4], graph pre-training for GAD can be further interpreted as a regression problem in the form of $\sigma(\boldsymbol{\alpha}) = \sigma(g(\Lambda)\boldsymbol{\beta})$.

Note that $\hat{\mathbf{X}}$ is fully determined by graph filter $g(\cdot)$, we consider the Spectral Regression Loss (SRL) [23] as the evaluation metric of the filter function:

$$\mathcal{L}(\mathcal{G}) = \sum_{i=1}^n \left(\frac{\alpha_i}{\sqrt{n}} - \frac{g(\lambda_i)\beta_i}{\sqrt{\sum_{j=1}^n g(\lambda_j)^2 \beta_j^2}} \right)^2, \quad (4)$$

By definition, a graph filter $g(\cdot)$ that achieves **lower** SRL is of **higher** performance in binary classification tasks like GAD [23], and a corresponding proposition is presented below:

PROPOSITION 2. *For a binary graph anomaly detection problem, a low-pass filter will get a larger SRL $\mathcal{L}(\mathcal{G})$ and poorer performance as the heterophily of abnormal nodes increases. In this case, incorporating a high-pass filter can lower the upper bound of SRL.*

We provide proofs and detailed discussions in Appendix B.2. Proposition 2 establishes the limitations of low-pass filters and underscores the necessity of incorporating high-pass filters, particularly in the context of graph pre-training with nodes having high heterophily, as encountered in GAD. Motivated by the analyses above, to better accommodate the mixed homophily-heterophily pattern exhibited in GAD, a natural idea is to use an additional high-pass filter alongside the conventional low-pass filter to capture information across the entire frequency spectrum.

3.2 Expressiveness of Spectral Filtering

The preceding analysis suggests the potential of introducing high-pass graph filters to deal with the mixed homophily-heterophily pattern. In this subsection, we further present the theoretical justification for the necessity of selectively applying low- and high-pass filters to individual nodes, accompanied by a toy example for easy illustration.

Our theoretical analysis is based on the Contextual Stochastic Block Model (CSBM) [7], which is a generative model for attributed graphs that has been widely applied in graph analysis [1, 13, 33, 34, 47]. To reflect GAD's dual natures, namely, imbalanced binary classification and the coexistence of homophilic and heterophilic structures, we first introduce the Anomalous Stochastic Block Model (ASBM) to describe the anomaly detection graphs. Essentially, ASBM integrates two CSBMs, where one accounts for the homophilic pattern while the other characterizes the heterophilic relationships. The formal definition is presented as follows:

DEFINITION 1 (ANOMALOUS STOCHASTIC BLOCK MODEL). *An **Anomalous Stochastic Block Model** is a generative model for attributed anomaly detection graphs, denoted as $\text{ASBM}(n_a, n_n, \boldsymbol{\mu}, \boldsymbol{\nu}, (p_1, q_1), (p_2, q_2), P_a, P_n)$. It generates two sets of nodes: abnormal nodes C_a and normal nodes C_n , where $|C_a| = n_a$ and $|C_n| = n_n$. For abnormal (normal) nodes, each row of the feature matrix $\mathbf{X}_a \in \mathbb{R}^{n_a \times d}$ ($\mathbf{X}_n \in \mathbb{R}^{n_n \times d}$) is sampled from a d -dimensional Gaussian distribution $N(\boldsymbol{\mu}, \frac{1}{d} \mathbf{I})$ ($N(\boldsymbol{\nu}, \frac{1}{d} \mathbf{I})$), where $\boldsymbol{\mu}, \boldsymbol{\nu}$ are the fixed class mean vectors with $\|\boldsymbol{\mu}\|_2, \|\boldsymbol{\nu}\|_2 \leq 1$, and \mathbf{I} is the identity matrix. The full feature matrix \mathbf{X} is obtained by stacking $[\mathbf{X}_a, \mathbf{X}_n]$.*

Abnormal and normal nodes are in a homophilic pattern with the probabilities of P_a and P_n , respectively. The homophilic pattern is generated with intra-class and inter-class edge probability $p_1 > q_1$: for nodes v_i in the homophilic pattern, the edge e_{ij} follows a

Bernoulli distribution, $e_{ij} \sim \text{Ber}(p_1)$ if v_i and v_j are in the same class, and $e_{ij} \sim \text{Ber}(q_1)$ if they are in distinct classes. In contrast, the heterophilic pattern is generated with $p_2 < q_2$. Therefore, both abnormal and normal nodes consist of two subgroups: 1) C_a^1, C_n^1 for nodes exhibiting a homophilic pattern; 2) C_a^2, C_n^2 for nodes exhibiting a heterophilic pattern.

For simplicity, let $\mathcal{H}_o = C_a^1 \cup C_n^1$ and $\mathcal{H}_e = C_a^2 \cup C_n^2$ denote the homophilic and heterophilic node sets, respectively. We assume that the nodes follow the same degree distribution with $p_1 + q_1 = p_2 + q_2$.

To assess the impact of different spectral filters on ASBM, following [1, 13], we consider a linear model with parameters $w \in \mathbb{R}^d$ and $b \in \mathbb{R}$. The predicted labels are given by $\hat{y} = \sigma(\hat{X}w + b)$, where $\sigma(\cdot)$ is the sigmoid function and $\hat{X} = Ug(\Lambda)U^\top X$ is the filtered feature. The loss function used is the binary cross entropy as in Eq. (12). The separability of the linear model adheres to the following theorem:

THEOREM 1. Assume the graph size $n = n_a + n_n$ is relatively large with $\omega(d \log d) \leq n \leq O(\text{poly}(d))$, the graph is not too sparse with $p_1, q_1, p_2, q_2 = \omega(\log^2(n)/n)$, the feature center distance is not too small with $\|\mu - \nu\| = \Omega(\frac{\log n}{\sqrt{dn(p_1+q_1)}})$, the sizes of the homophilic and heterophilic node sets are approximately equal, and $\|w\| \leq R$. For the graph $\mathcal{G}(\mathcal{V}, \mathcal{E}, X) \sim \text{ASBM}(n_a, n_n, \mu, \nu, (p_1, q_1), (p_2, q_2), P_a, P_n)$, when low- and high-pass filters are applied separately to the homophilic and heterophilic node sets $\mathcal{H}_o, \mathcal{H}_e$, respectively, there exists an optimal w^*, b^* such that all nodes are linearly separable with the following probability:

$$\mathbb{P}\left(\left(\hat{X}_i\right)_{i \in \mathcal{V}^L} \text{ is linearly separable}\right) = 1 - o_d(1), \quad (5)$$

where $o_d(1)$ denotes a quantity that converges to 0 as $d \rightarrow \infty$.

The proof is provided in Appendix B.3. Theorem 1 demonstrates that by applying low- and high-pass filters separately to nodes with different homophily levels, it is possible to achieve linear separability for all nodes.

For empirical illustration, we further present a toy example in Figure 2, where node labels are indicated by colors. Nodes $\{1, 2, 3, 5\}$ exhibit heterophilic patterns, having more neighbors with different labels, while nodes $\{4, 6, 7\}$ exhibit homophilic patterns, having more neighbors with the same label. As demonstrated, applying a global low- or high-pass filter to all nodes results in indistinguishability, meaning no split point can perfectly classify the nodes. For instance, if set the split point to 0, applying the global low-pass filter $D^{-1/2}AD^{-1/2}$ erroneously places the abnormal nodes $\{1, 2, 3\}$ into the normal set, and the normal node 5 into the abnormal set. Similarly, applying the global high-pass filter $-D^{-1/2}AD^{-1/2}$ results in normal nodes $\{4, 6, 7\}$ being classified as anomalies. However, when the low- and high-pass filters are applied separately to the homophilic nodes $\{4, 6, 7\}$ and the heterophilic nodes $\{1, 2, 3, 5\}$, all nodes can be correctly classified. Overall, our findings highlight the potential of applying appropriate filters to individual nodes in handling the mixed homophily-heterophily pattern in GAD.

4 Methodology

Motivated by the analysis in Section 3, we introduce PAF, a Pre-training and Adaptive Fine-tuning framework specifically designed

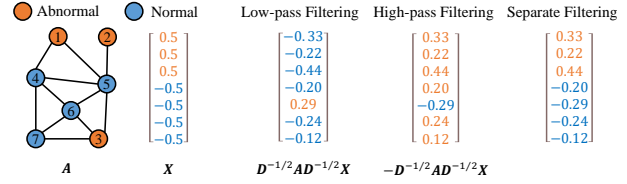


Figure 2: An example to illustrate the effects of low-pass, high-pass, and separate filtering. While applying a global low- or high-pass filter to all nodes results in indistinguishability, using separate filtering can achieve linear separability for all nodes.

for GAD, which involves two stages: (1) **Low-&High-Pass Filter Pre-Training** and (2) **Node-&Dimension-Adaptive Fine-Tuning**. The overall PAF framework is illustrated in Figure 3.

4.1 Low-&High-Pass Filter Pre-Training

Previous graph pre-training methods [16, 29, 44, 46, 55] are primarily based on the homophily assumption, utilizing a low-pass filter (e.g., GCN [21]) to learn node representations. However, in GAD, abnormal nodes typically exhibit higher heterophily compared to normal nodes (see Figure 1 and Table 3). To address this, Theorem 1 provides a theoretical guideline: applying low- and high-pass filters separately to homophilic and heterophilic nodes. Accordingly, we propose to jointly train a low-pass graph encoder $f_l(\cdot)$ and a high-pass graph encoder $f_h(\cdot)$ in the pre-training phase using a task-irrelevant self-supervised objective \mathcal{L}_{pt} :

$$\min_{f_l, f_h} \mathcal{L}_{pt}(f_l(\mathcal{G}), f_h(\mathcal{G})). \quad (6)$$

By utilizing $f_l(\cdot)$ and $f_h(\cdot)$, our graph encoders can acquire both low- and high-frequency information of node features, preserving critical heterophily and anomaly information in addition to the underlying structural and relational patterns of the graph [6, 50].

Instantiation. Here, we present an instantiation of the pre-training phase. In particular, we utilize the symmetric normalized adjacency matrix $D^{-1/2}AD^{-1/2}$ [21] as the low-pass filter F_L for low-pass graph encoder $f_l(\cdot)$. For the high-pass graph encoder $f_h(\cdot)$, we set the high-pass filter $F_H = I - D^{-1/2}AD^{-1/2}$. Mathematically, the k -layer $f_l(\cdot)$ and $f_h(\cdot)$ can be expressed as:

$$\begin{aligned} Z_L &= F_L \sigma \left(\cdots \sigma \left(F_L X W_L^0 \right) \cdots \right) W_L^{k-1}, \\ Z_H &= F_H \sigma \left(\cdots \sigma \left(F_H X W_H^0 \right) \cdots \right) W_H^{k-1}, \end{aligned} \quad (7)$$

where $Z_L, Z_H \in \mathbb{R}^{n \times e}$ represent the low- and high-pass node representations, respectively. $\sigma(\cdot)$ denotes the activation function, W_L^i and W_H^i are the corresponding learnable weight matrices.

For the optimization objective of $f_l(\cdot)$ and $f_h(\cdot)$, we adopt the Deep Graph Infomax (DGI) [46] due to its effectiveness and computational efficiency, with linear time and space complexity relative to the graph size. DGI aims to maximize the mutual information between local patches (node representations) and the global summary representation of the entire graph. Given the low- and high-pass node representations Z_L and Z_H , the global low- and

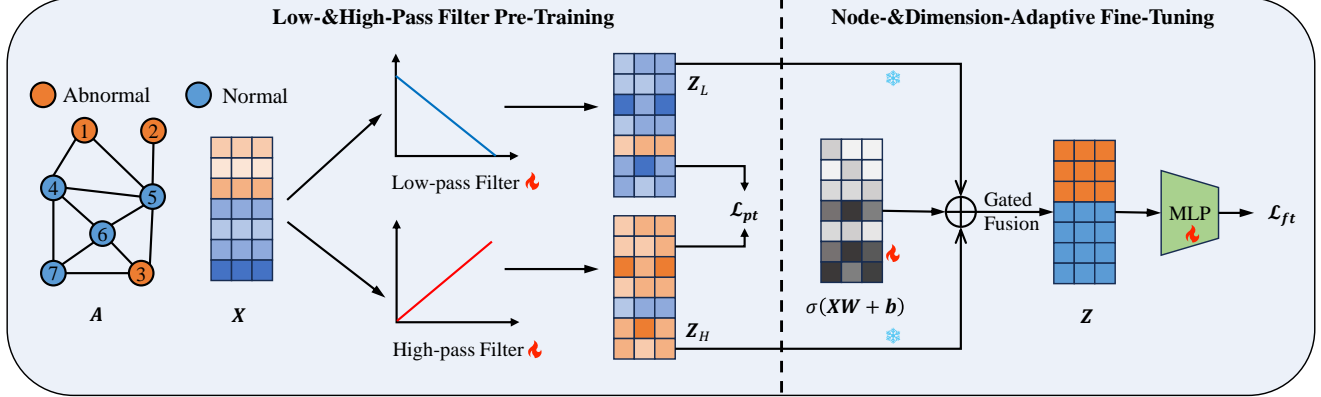


Figure 3: Overview of our proposed PAF. We first train two separate low- and high-pass filters to retain the low- and high-frequency components of node features, respectively. Subsequently, we fine-tune an MLP-based classifier in a node- and dimension-adaptive manner, enabling automatic selection of the most appropriate frequency information for different nodes.

high-pass summary representations can be obtained by mean pooling as $s^L = \frac{1}{n} \sum_{i=1}^n Z_i^L$ and $s^H = \frac{1}{n} \sum_{i=1}^n Z_i^H$. In the meantime, we randomly shuffle X and pass it through $f_l(\cdot)$ and $f_h(\cdot)$ to generate the negative low- and high-pass node representations \tilde{Z}_L and \tilde{Z}_H . Subsequently, we maximize the mutual information between node representations and global graph summaries using a noise-contrastive objective with binary cross-entropy loss:

$$\begin{aligned} \mathcal{L}_{pt} = & -\frac{1}{n} \sum_i^n \left(\log \mathcal{D}(Z_i^L, s^L) + \log (1 - \mathcal{D}(\tilde{Z}_i^L, s^L)) \right) \\ & -\frac{1}{n} \sum_i^n \left(\log \mathcal{D}(Z_i^H, s^H) + \log (1 - \mathcal{D}(\tilde{Z}_i^H, s^H)) \right), \end{aligned} \quad (8)$$

where $\mathcal{D}(z, s) = \text{Sigmoid}(z^T W s) \in [0, 1]$ is the discriminator parameterized by a learnable weight matrix W , aiming to distinguish negative node representations from original ones. In addition to DGI, we can also use other self-supervised pretext objectives, such as InfoNCE [12, 57] and Barlow Twins [2, 54]. Further details can be found in Appendix C.

4.2 Node-&Dimension-Adaptive Fine-Tuning

During the fine-tuning phase, we aim to train an MLP-based classifier using the pre-trained low- and high-pass node representations $Z_L, Z_H \in \mathbb{R}^{n \times e}$, with a small set of labeled normal and abnormal nodes. As per Theorem 1, selecting the most appropriate frequency information for individual nodes is crucial. Thus, we seek to learn a node-adaptive aggregation mechanism that selectively combines low- and high-frequency information from Z_L and Z_H for individual nodes. Additionally, as suggested by [11, 49], the importance of different feature dimensions/channels usually varies, and thus the aggregation mechanism should also be dimension-adaptive. To this end, we propose to learn a coefficient matrix $C \in [0, 1]^{n \times e}$ to aggregate Z_L and Z_H as follows:

$$Z = C \odot Z_L + (1 - C) \odot Z_H, \quad (9)$$

where \odot is the Hadamard product, and Z represents the resulting node representations, which are subsequently fed into the classifier. To learn C , one might treat it as free parameters to be directly optimized [49]. However, several concerns arise with this approach: 1) The size of C is proportional to both the number of nodes and feature dimensions, leading to a large number of parameters that must be learned. 2) As shown in Eq. (12), only the gradients from y_i can update the parameters C_i corresponding to node i , which makes C is difficult to optimize efficiently, particularly in our case where the number of labeled nodes is small. 3) Directly learning C neglects the input node features, which typically offer valuable information beneficial for GAD [42].

To address these issues, we propose to use a gated fusion network (GFN) to generate node- and dimension-specific coefficients. Specifically, based on the node features X , GFN generates a unique coefficient vector for each node as follows:

$$C = \sigma(XW + b), \quad (10)$$

where $\sigma(\cdot)$ is the sigmoid function, $W \in \mathbb{R}^{d \times e}$ is a learnable transformation matrix, and $b \in \mathbb{R}^e$ is a bias vector. Since abnormal nodes require greater access to high-frequency information compared to normal nodes, we further introduce a regularization term to guide the generation of C . Treating $c_i = \frac{1}{e} \sum_{j=1}^e C_{ij}$ as the mean preference of node i for low-frequency information, we aim to ensure that c_i for abnormal nodes approaches $p^a \in [0, 1]$, while for normal nodes, it approaches $p^n \in [0, 1]$. The regularization term is formulated as a binary cross-entropy loss:

$$\begin{aligned} \mathcal{L}_{reg} = & -\frac{1}{|\mathcal{V}^L|} \sum_{i \in \mathcal{V}^L \wedge y_i=1} p^a \log(c_i) + (1 - p^a) \log(1 - c_i) \\ & -\frac{1}{|\mathcal{V}^L|} \sum_{i \in \mathcal{V}^L \wedge y_i=0} p^n \log(c_i) + (1 - p^n) \log(1 - c_i), \end{aligned} \quad (11)$$

where p^a and p^n are hyperparameters with the constraint $p^a \leq p^n$ to encourage abnormal nodes to exploit more high-frequency information. The benefits of using GFN are clear and significant.

First, it reduces the parameter complexity of C from $O(n \times e)$ to $O((d+1) \times e)$, where e and d are much smaller than n . Second, GFN improves the optimization process. Instead of relying solely on \mathbf{y}_i to optimize C_i , it introduces a learnable transformation matrix \mathbf{W} that adaptively estimates the coefficient matrix, thereby addressing the optimization challenge. Third, the generated C also encapsulates raw node features, providing richer information for fine-tuning. With such C , we obtain the combined node representations Z via Eq. (9). Then we feed Z into a two-layer MLP to generate the prediction \hat{y}_i for each labeled node i and optimize the parameters using the binary cross-entropy loss:

$$\mathcal{L}_{bce} = -\frac{1}{|\mathcal{V}^L|} \sum_{i \in \mathcal{V}^L} y_i \log(\hat{y}_i) + (1 - y_i) \log(1 - \hat{y}_i). \quad (12)$$

Finally, we have the overall fine-tuning loss by combining the classification loss and the regularization loss:

$$\mathcal{L}_{ft} = \mathcal{L}_{bce} + \mathcal{L}_{reg} \quad (13)$$

5 Experiments

In this section, we conduct comprehensive experiments and answer the following research questions: **RQ1**: How does PAF compare to state-of-the-art GAD and graph pre-training baselines? **RQ2**: How to visually understand the learned node- & dimension-wise coefficients? **RQ3**: Do our low- & high-pass filter pre-training and node- & dimension-adaptive fine-tuning contribute positively to GAD? **RQ4**: How does PAF perform with different numbers of labels? **RQ5**: How do hyperparameters influence the performance of PAF?

5.1 Experimental Setup

Datasets. Following GADBench [42], we conduct experiments on 10 real-world datasets spanning various scales and domains: Reddit [22], Weibo [22], Amazon [35], YelpChi [41], T-Finance [43], Elliptic [51], Tolokers [37], Questions [37], DGraph-Fin [17], and T-Social [43]. Dataset statistics are presented in Table 3 and descriptions of these datasets are provided in Appendix E.1.

Baselines. We compare our model with a series of baseline methods, which can be categorized into the following groups: Standard GNN Architectures, including GCN [21], GIN [53], GAT [45]; GNNs Specialized for GAD, including PCGNN [25], BernNet [14], AM-Net [3], BWGNN [43], GHRN [10], and ConsisGAD [5]; Graph Pre-Training Methods, including DGI [46], GRACE [57], DCI [50], BGRL [44], GraphMAE [16], G-BT [2], SSGE [27], and PolyGCL [4]. Note that PolyGCL and our proposed PAF jointly pre-train low- and high-pass filters, while others pre-train only a low-pass filter GCN. Details of these baselines are in Appendix E.2.

Evaluation Protocols. Following GADBench [42], we evaluate performance using three popular metrics: the Area Under the Receiver Operating Characteristic Curve (AUROC), the Area Under the Precision-Recall Curve (AUPRC) calculated via average precision, and the Recall score within the top- K predictions (Rec@K). Here, K corresponds to the number of anomalies in the test set. For all metrics, anomalies are treated as the positive class, with higher scores indicating better model performance. To closely simulate real-world scenarios with limited supervision, we standardize the training/validation set across all datasets to include 100 labels—20

positive (abnormal) and 80 negative (normal) labels [42]. To ensure the robustness of our findings, we perform 10 random splits, as provided by [42], on each dataset and report the average performance.

Implementation Details. For all baseline methods, we use the implementations provided by GADBench [42] or the respective authors. Our PAF is implemented using PyTorch and the Deep Graph Library [48]. Due to space constraints, hyperparameter details are provided in Appendix E.2.4. To facilitate reproducibility, our code is open-sourced at <https://anonymous.4open.science/r/PAF-163E>.

5.2 Performance Comparison (RQ1)

We present a comprehensive comparison of performance across 10 benchmark datasets. The AUROC, AUPRC, and Rec@K results are shown in Table 1, Table 4, and Table 5, respectively. As observed, existing pre-training methods have shown promising results on several benchmark datasets such as Reddit and Tolokers. However, their performance on the Amazon and YelpChi datasets has been notably underwhelming, often falling far behind the end-to-end GAD baselines. This discrepancy suggests that relying solely on a low-pass filter does not universally fit all graph structures. In contrast, our proposed PAF demonstrates superior performance, achieving state-of-the-art results in most cases. For instance, PAF shows average AUROC improvements of 5.2%, 4.0%, and 3.3% over DGI, G-BT, and GRACE; AUPRC improvements of 11.8%, 11.1%, and 8.6% over DGI, G-BT, and GRACE; and Rec@K improvements of 10.2%, 8.6%, and 6.9% over DGI, G-BT, and GRACE, respectively. On the Amazon, YelpChi, DGraph-Fin, and T-Social datasets, PAF exhibits the leading performance and outperforms other GNN and GAD baselines by 1.7%, 2.1%, 3.5%, and 1.8% AUROC, respectively. These results underline the importance of jointly pre-training both low- and high-pass filters, as this combination enables the model to retain sufficient information for detecting anomalies.

5.3 Visualization of Coefficients (RQ2)

To gain visual insights into PAF, we present heatmaps that depict the learned coefficients C . The results for DGI+PAF are presented in Figure 4, while the results for G-BT+PAF and GRACE+PAF are deferred to Figures 8 and 9 in the appendix. For clarity, we focus on the top 8 dimensions of C for 3 randomly selected abnormal nodes a_1, a_2, a_3 and 3 randomly selected normal nodes n_1, n_2, n_3 . As illustrated, these coefficients are personalized for each node, verifying that each node has its own set of learned coefficients, which vary across dimensions. For Amazon, T-Finance, and Tolokers, abnormal nodes generally have lower coefficients than normal nodes, consistent with the expectation that abnormal nodes require more high-frequency information. For Weibo, the coefficient distributions for abnormal and normal nodes are similar, which is attributed to the minor difference in their node homophily ratios. Furthermore, the learned coefficients are dimension-specific, meaning the aggregation of low- and high-frequency representations varies across dimensions for each node. This enables fine-grained aggregation that reflects the importance of specific frequency bands in each dimension of the node representations.

Table 1: Comparison of AUROC for each model. “-” denotes “out of memory”.

Model	Reddit	Weibo	Amazon	Yelp.	T-Fin.	Ellip.	Tolo.	Quest.	DGraph.	T-Social
GCN	56.9 \pm 5.9	93.5 \pm 6.6	82.0 \pm 0.3	51.2 \pm 3.7	88.3 \pm 2.5	86.2 \pm 1.9	64.2 \pm 4.8	60.0 \pm 2.2	66.2 \pm 2.5	71.6 \pm 10.4
GIN	60.0 \pm 4.1	83.8 \pm 8.3	91.6 \pm 1.7	62.9 \pm 7.3	84.5 \pm 4.5	88.2 \pm 0.9	66.8 \pm 5.2	62.2 \pm 2.2	65.7 \pm 1.8	70.4 \pm 7.4
GAT	60.5 \pm 3.9	86.4 \pm 7.7	92.4 \pm 1.9	65.6 \pm 4.0	85.0 \pm 4.5	88.5 \pm 2.1	68.1 \pm 3.0	62.3 \pm 1.4	67.2 \pm 1.9	75.4 \pm 4.8
PCGNN	52.8 \pm 3.4	83.9 \pm 8.1	93.2 \pm 1.2	65.1 \pm 4.8	92.0 \pm 1.1	87.5 \pm 1.4	67.4 \pm 2.1	59.0 \pm 4.0	68.4 \pm 4.2	69.1 \pm 2.4
BernNet	63.1 \pm 1.7	80.1 \pm 6.9	92.1 \pm 2.4	65.0 \pm 3.7	91.2 \pm 1.0	87.0 \pm 1.7	61.9 \pm 5.6	61.8 \pm 6.4	69.0 \pm 1.4	59.8 \pm 6.3
AMNet	62.9 \pm 1.8	82.4 \pm 4.6	92.8 \pm 2.1	64.8 \pm 5.2	92.6 \pm 0.9	85.4 \pm 1.7	61.7 \pm 4.1	63.6 \pm 2.8	67.1 \pm 3.2	53.7 \pm 3.4
BWGNN	57.7 \pm 5.0	93.6 \pm 4.0	91.8 \pm 2.3	64.3 \pm 3.4	92.1 \pm 2.7	88.7 \pm 1.3	68.5 \pm 2.7	60.2 \pm 8.6	65.5 \pm 3.1	77.5 \pm 4.3
GHRN	57.5 \pm 4.5	91.6 \pm 4.4	90.9 \pm 1.9	64.5 \pm 3.1	92.6 \pm 0.7	89.0 \pm 1.3	69.0 \pm 2.2	60.5 \pm 8.7	67.1 \pm 3.0	78.7 \pm 3.0
ConsisGAD	59.6 \pm 2.8	85.0 \pm 3.7	92.3 \pm 2.2	66.1 \pm 3.8	94.3 \pm 0.8	88.6 \pm 1.3	68.5 \pm 2.0	65.7 \pm 3.9	67.1 \pm 3.0	93.1 \pm 1.9
DCI	61.0 \pm 3.1	89.3 \pm 5.3	89.4 \pm 3.0	64.1 \pm 5.3	88.0 \pm 3.2	88.5 \pm 1.3	67.6 \pm 7.1	62.2 \pm 2.5	65.3 \pm 2.3	74.2 \pm 3.3
GraphMAE	61.0 \pm 0.5	95.7 \pm 2.3	84.2 \pm 0.3	55.2 \pm 0.3	91.4 \pm 0.7	82.5 \pm 1.4	66.3 \pm 3.0	62.5 \pm 1.4	63.7 \pm 1.6	89.2 \pm 4.5
BGRL	65.3 \pm 2.2	99.0 \pm 0.5	84.3 \pm 1.0	57.0 \pm 1.2	88.0 \pm 1.7	88.5 \pm 1.7	72.0 \pm 1.8	65.7 \pm 2.9	64.9 \pm 1.6	90.2 \pm 1.3
SSGE	62.2 \pm 4.7	95.1 \pm 1.6	84.7 \pm 2.0	55.7 \pm 1.8	92.9 \pm 0.7	86.7 \pm 1.2	71.9 \pm 1.5	65.5 \pm 1.5	68.6 \pm 2.9	92.3 \pm 0.8
PolyGCL	62.7 \pm 3.9	97.4 \pm 0.6	93.3 \pm 1.3	65.1 \pm 4.1	89.3 \pm 0.6	87.9 \pm 0.9	68.1 \pm 1.8	64.8 \pm 3.8	67.4 \pm 2.0	91.4 \pm 1.5
DI	63.0 \pm 3.0	96.7 \pm 2.5	87.7 \pm 0.7	54.0 \pm 1.8	91.8 \pm 0.8	86.2 \pm 1.4	71.5 \pm 0.7	68.7 \pm 3.8	64.3 \pm 2.2	89.3 \pm 1.3
+PAF	66.1 \pm 2.0	98.6 \pm 0.2	94.9 \pm 1.0	68.2 \pm 1.6	94.7 \pm 0.2	90.8 \pm 1.1	73.5 \pm 1.3	71.8 \pm 2.4	72.0 \pm 0.3	94.9 \pm 1.4
Avg.\uparrow +5.2	+3.1	+1.9	+7.2	+14.2	+2.9	+4.6	+2.0	+3.1	+7.7	+5.6
G-BT	63.8 \pm 4.3	97.3 \pm 1.1	84.8 \pm 1.6	55.5 \pm 1.8	93.0 \pm 0.6	88.5 \pm 1.2	71.7 \pm 1.3	67.0 \pm 1.6	69.4 \pm 2.5	90.9 \pm 1.2
+PAF	66.7 \pm 4.0	98.1 \pm 0.7	93.8 \pm 1.6	68.2 \pm 2.3	94.2 \pm 0.7	91.5 \pm 1.1	72.7 \pm 1.3	69.8 \pm 1.5	72.5 \pm 0.9	94.8 \pm 1.9
Avg.\uparrow +4.0	+2.9	+0.8	+9.0	+12.7	+1.2	+3.0	+1.0	+2.8	+3.1	+3.9
GRACE	64.5 \pm 3.3	97.1 \pm 1.9	87.9 \pm 0.7	55.5 \pm 1.4	93.1 \pm 0.3	88.8 \pm 1.8	70.6 \pm 1.6	68.2 \pm 1.7	-	-
+PAF	67.2 \pm 4.1	98.2 \pm 0.7	93.4 \pm 1.1	66.2 \pm 3.2	94.3 \pm 0.4	90.7 \pm 1.2	73.1 \pm 1.2	69.0 \pm 4.4	-	-
Avg.\uparrow +3.3	+2.7	+1.1	+5.5	+10.7	+1.2	+1.9	+2.5	+0.8	-	-

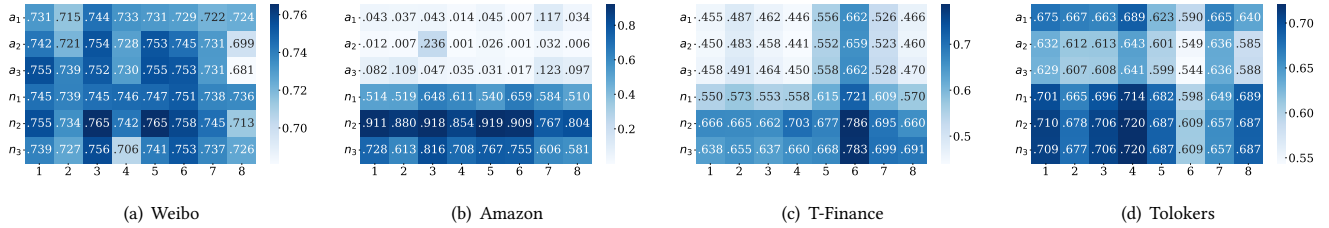


Figure 4: Visualization of the learned coefficients by the DGI+PAF model for the top 8 dimensions. The nodes a_1, a_2, a_3 are 3 randomly selected abnormal nodes, while n_1, n_2, n_3 are 3 randomly selected normal nodes.

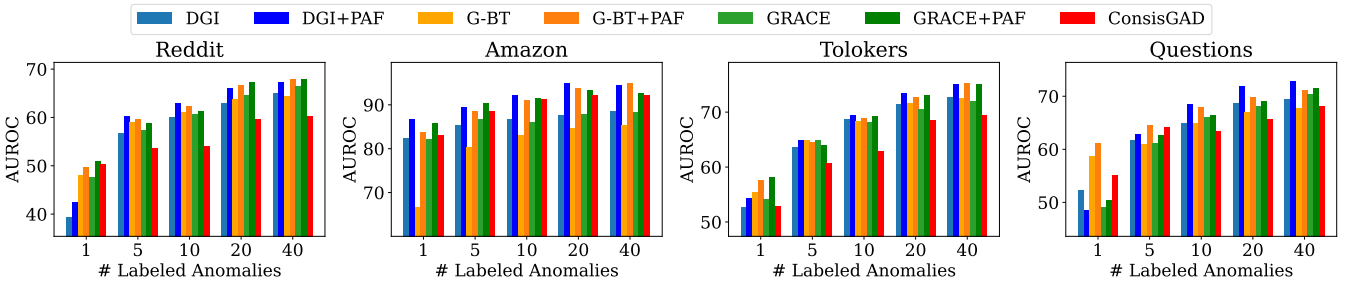
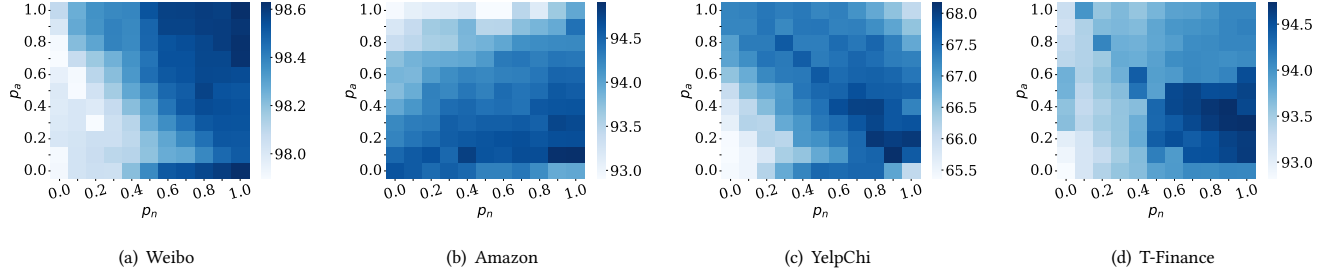
5.4 Ablation Study (RQ3)

We conduct an ablation study to evaluate the effectiveness of PAF from three key perspectives: Filtering, Aggregation, and Regularization. Specifically, we compare PAF with eight variants, where “NDAdpt” represents our node- and dimension-adaptive representation aggregation method; “Mean”, “Concat”, “Scalar”, “Vector”, and “Atten.” refer to different aggregation strategies for combining low- and high-pass node representations; “Low” and “High” use only the low-pass node representations Z_L or the high-pass node representations Z_H , respectively. The mathematical formulations of them are described in Appendix D. The results for DGI+PAF are presented in Table 2, and the results for the other two models are provided in Tables 6 and 7. It is observed that: 1) **Filtering**: Using

both low- and high-frequency information generally yields better performance than relying on only one, highlighting the importance of pre-training both low- and high-pass filters for GAD tasks. 2) **Aggregation**: Our node- and dimension-adaptive strategy consistently outperforms or is at least competitive with these alternatives, demonstrating the benefits of incorporating both frequency-selective information and node-specific adaptation. 3) **Regularization**: The regularization term \mathcal{L}_{reg} further enhances the model’s ability to distinguish between normal and abnormal nodes by encouraging abnormal nodes to rely more on high-frequency information, leading to additional performance gains.

Table 2: Ablation study on each component of our PAF. The backbone is DGI+PAF.

Variants				YelpChi			Elliptic			Questions			DGraph-Fin		
Z_L	Z_H	\mathcal{L}_{reg}	Aggr.	AUROC	AUPRC	Rec@K	AUROC	AUPRC	Rec@K	AUROC	AUPRC	Rec@K	AUROC	AUPRC	Rec@K
✓	✓	✓	NDAp	68.2±1.6	27.1±1.6	30.4±1.6	90.8±1.1	59.4±4.7	62.1±2.3	71.8±2.4	12.2±1.3	16.5±0.8	72.0±0.3	2.9±0.0	4.0±0.1
✓	✓	✗	NDAp	67.6±1.4	26.6±1.5	29.8±1.2	90.8±1.1	59.4±4.9	61.7±2.9	71.2±2.7	11.1±1.6	15.9±0.9	71.7±0.4	2.8±0.1	3.7±0.2
✓	✓	✗	Mean	67.1±1.5	26.3±1.7	29.4±1.6	87.8±1.5	49.9±4.1	52.5±2.1	71.0±2.4	10.8±1.7	15.7±1.2	71.6±0.4	2.8±0.1	3.8±0.2
✓	✓	✗	Concat	65.5±2.5	25.2±2.3	28.3±2.2	88.1±1.5	50.5±4.6	53.3±3.2	68.5±3.2	11.1±1.5	15.2±1.7	71.5±0.2	2.8±0.0	3.6±0.3
✓	✓	✗	Scalar	66.6±1.4	25.7±1.5	28.8±1.5	87.9±1.6	50.7±4.2	53.1±1.9	70.7±2.7	10.7±1.6	15.7±1.1	71.5±0.4	2.8±0.1	3.8±0.2
✓	✓	✗	Vector	67.1±1.6	26.3±1.7	29.5±1.6	87.5±1.2	49.9±4.4	52.1±2.1	71.2±2.5	10.9±1.8	16.0±1.4	71.5±0.4	2.8±0.0	3.7±0.2
✓	✓	✗	Atten.	66.7±1.7	26.2±1.6	29.5±1.7	86.0±2.4	43.4±7.0	48.8±6.0	67.5±3.5	8.3±2.2	13.6±2.6	71.7±0.3	2.8±0.0	3.8±0.2
✓	✗	✗	Low	55.6±1.4	17.9±1.2	20.6±1.7	87.1±1.7	43.8±3.2	47.9±3.6	70.6±1.2	11.8±1.2	16.4±0.9	67.9±1.0	2.5±0.1	4.0±0.1
✗	✓	✗	High	63.7±3.0	23.4±2.1	26.7±2.3	83.5±1.6	36.3±6.8	42.5±5.9	66.1±3.2	6.3±0.7	9.8±1.9	71.1±0.5	2.6±0.1	3.1±0.5

**Figure 5: How the AUROC score varies with different numbers of labeled anomalies.****Figure 6: How the AUROC score of DGI+PAF varies with different values of p_a and p_n .**

5.5 Under Varying Supervision (RQ4)

This section evaluates the performance of PAF under varying levels of supervision by modifying the number of labeled abnormal nodes. Following [42], the number of labeled normal nodes is set to four times the number of labeled abnormal nodes. We present the results in terms of AUROC, AUPRC, and Rec@K in Figures 5, 10, and 11, respectively. As expected, performance generally improves across all methods as the number of labeled nodes increases. Notably, PAF delivers consistent improvements over baseline pre-training methods and surpasses the current state-of-the-art, ConsisGAD, even with only a single labeled abnormal node. This highlights the effectiveness of our approach in addressing GAD with limited supervision.

5.6 Hyperparameter Analysis (RQ5)

Compared to previous graph pre-training methods, our PAF introduces two additional hyperparameters, p_a and p_n , which represent the expected preference for low-frequency information in abnormal and normal nodes, respectively. To assess their impact on model performance, we vary these hyperparameters from 0.0 to 1.0 in increments of 0.1. The results for DGI+PAF are presented in Figure 6, while the results for G-BT+PAF and GRACE+PAF are deferred to Figures 12 and 13 in the appendix. It is observed that the right half of the heatmap, corresponding to relatively larger p_n values, generally outperforms the left half, since normal nodes usually favor low-frequency information. Additionally, the optimal combination of (p_a, p_n) always appears in the lower-right half of the heatmap, where $p_a \leq p_n$, indicating the model assigns larger coefficients to the high-pass node representations for abnormal nodes.

This is in line with the expectation that abnormal nodes require more high-frequency information than normal nodes. Overall, PAF demonstrates robustness to p_a and p_n : by maintaining p_a and p_n within the appropriate range, PAF achieves impressive and competitive performance.

6 Conclusion

In this paper, we introduce PAF, a Pre-training and Adaptive Fine-tuning framework tailored for GAD. We theoretically examine the influence of mixed homophily-heterophily patterns on graph pre-training and demonstrate the potential of applying suitable filters to individual nodes. Building on this analysis, PAF trains two separate low- and high-pass filters to capture both low- and high-frequency information in node features. During fine-tuning, PAF employs a gated fusion network to help fine-tune an MLP-based classifier in a node- and dimension-adaptive manner, enabling automatic selection of the most relevant frequency information for different nodes. Extensive experiments show that PAF achieves state-of-the-art performance in GAD with limited supervision.

Acknowledgments

We would like to express our sincere gratitude to the reviewers and chairs for their invaluable time and effort dedicated to the evaluation of our manuscript.

References

- [1] Aseem Baranwal, Kimon Fountoulakis, and Aukosh Jagannath. 2021. Graph Convolution for Semi-Supervised Classification: Improved Linear Separability and Out-of-Distribution Generalization. In *International Conference on Machine Learning*. PMLR, 684–693.
- [2] Piotr Bielak, Tomasz Kajdanowicz, and Nitesh V Chawla. 2022. Graph barlow twins: A self-supervised representation learning framework for graphs. *Knowledge-Based Systems* 256 (2022), 109631.
- [3] Ziwei Chai, Siqi You, Yang Yang, Shiliang Pu, Jiarong Xu, Haoyang Cai, and Weihao Jiang. 2022. Can abnormality be detected by graph neural networks? In *IJCAI*. 1945–1951.
- [4] Jingyu Chen, Runlin Lei, and Zhewei Wei. 2024. PolyGCL: GRAPH CONTRASTIVE LEARNING via Learnable Spectral Polynomial Filters. In *The Twelfth International Conference on Learning Representations*.
- [5] Nan Chen, Zemin Liu, Bryan Hooi, Bingsheng He, Rizal Fathony, Jun Hu, and Jia Chen. 2024. Consistency Training with Learnable Data Augmentation for Graph Anomaly Detection with Limited Supervision. In *The Twelfth International Conference on Learning Representations*.
- [6] Jiashun Cheng, Zinan Zheng, Yang Liu, Jianheng Tang, Hongwei Wang, Yu Rong, Jia Li, and Fugee Tsung. 2024. Graph Pre-Training Models Are Strong Anomaly Detectors. *arXiv preprint arXiv:2410.18487* (2024).
- [7] Yash Deshpande, Subhabrata Sen, Andrea Montanari, and Elchanan Mossel. 2018. Contextual stochastic block models. *Advances in Neural Information Processing Systems* 31 (2018).
- [8] Kaize Ding, Jundong Li, Rohit Bhanushali, and Huan Liu. 2019. Deep anomaly detection on attributed networks. In *Proceedings of the 2019 SIAM international conference on data mining*.
- [9] Yingtong Dou, Zhiwei Liu, Li Sun, Yutong Deng, Hao Peng, and Philip S Yu. 2020. Enhancing graph neural network-based fraud detectors against camouflaged fraudsters. In *Proceedings of the 29th ACM international conference on information & knowledge management*. 315–324.
- [10] Yuan Gao, Xiang Wang, Xiangnan He, Zhenguang Liu, Huamin Feng, and Yongdong Zhang. 2023. Addressing heterophily in graph anomaly detection: A perspective of graph spectrum. In *Proceedings of the ACM Web Conference 2023*. 1528–1538.
- [11] Yuhe Guo and Zhewei Wei. 2023. Graph neural networks with learnable and optimal polynomial bases. In *International Conference on Machine Learning*.
- [12] Michael Gutmann and Aapo Hyvärinen. 2010. Noise-contrastive estimation: A new estimation principle for unnormalized statistical models. In *Proceedings of the thirteenth international conference on artificial intelligence and statistics*. 297–304.
- [13] Haoyu Han, Juanhui Li, Wei Huang, Xianfeng Tang, Hanqing Lu, Chen Luo, Hui Liu, and Jiliang Tang. 2024. Node-wise Filtering in Graph Neural Networks: A Mixture of Experts Approach. *arXiv preprint arXiv:2406.03464* (2024).
- [14] Mingguo He, Zhewei Wei, Hongteng Xu, et al. 2021. Bernnet: Learning arbitrary graph spectral filters via bernstein approximation. *Advances in Neural Information Processing Systems* 34 (2021), 14239–14251.
- [15] R Devon Hjelm, Alex Fedorov, Samuel Lavoie-Marchildon, Karan Grewal, Phil Bachman, Adam Trischler, and Yoshua Bengio. 2019. Learning deep representations by mutual information estimation and maximization. In *International Conference on Learning Representations*.
- [16] Zhenyu Hou, Xiao Liu, Yukuo Cen, Yuxiao Dong, Hongxia Yang, Chunjie Wang, and Jie Tang. 2022. Graphmae: Self-supervised masked graph autoencoders. In *Proceedings of the 28th ACM SIGKDD Conference on Knowledge Discovery and Data Mining*. 594–604.
- [17] Xuanwen Huang, Yang Yang, Yang Wang, Chunping Wang, Zhisheng Zhang, Jiarong Xu, Lei Chen, and Michalis Vazirgiannis. 2022. Dgraph: A large-scale financial dataset for graph anomaly detection. *Advances in Neural Information Processing Systems* (2022).
- [18] Yihong Huang, Liping Wang, Fan Zhang, and Xuemin Lin. 2023. Unsupervised graph outlier detection: Problem revisit, new insight, and superior method. In *2023 IEEE 39th International Conference on Data Engineering (ICDE)*.
- [19] Wei Ju, Siyu Yi, Yifan Wang, Qingqing Long, Junyu Luo, Zhiping Xiao, and Ming Zhang. 2024. A Survey of Data-Efficient Graph Learning. In *Proceedings of the Thirty-Third International Joint Conference on Artificial Intelligence, IJCAI-24*.
- [20] Diederik P. Kingma and Jimmy Ba. 2015. Adam: A Method for Stochastic Optimization. In *ICLR*.
- [21] Thomas N. Kipf and Max Welling. 2017. Semi-Supervised Classification with Graph Convolutional Networks. In *International Conference on Learning Representations*.
- [22] Srijan Kumar, Xikun Zhang, and Jure Leskovec. 2019. Predicting dynamic embedding trajectory in temporal interaction networks. In *Proceedings of the 25th ACM SIGKDD international conference on knowledge discovery & data mining*. 1269–1278.
- [23] Runlin Lei, Zhen Wang, Yaliang Li, Bolin Ding, and Zhewei Wei. 2022. Evennet: Ignoring odd-hop neighbors improves robustness of graph neural networks. *Advances in Neural Information Processing Systems* 35 (2022), 4694–4706.
- [24] Kay Liu, Yingtong Dou, Yue Zhao, Xueying Ding, Xiyang Hu, Ruitong Zhang, Kaize Ding, Canyu Chen, Hao Peng, Kai Shu, et al. 2022. BOND: Benchmarking unsupervised outlier node detection on static attributed graphs. *Advances in Neural Information Processing Systems* (2022).
- [25] Yang Liu, Xiang Ao, Zidi Qin, Jianfeng Chi, Jinghua Feng, Hao Yang, and Qing He. 2021. Pick and choose: a GNN-based imbalanced learning approach for fraud detection. In *Proceedings of the web conference 2021*. 3168–3177.
- [26] Yunhui Liu, Xinyi Gao, Tieke He, Tao Zheng, Jianhua Zhao, and Hongzhi Yin. 2024. Reliable node similarity matrix guided contrastive graph clustering. *IEEE Transactions on Knowledge and Data Engineering* (2024).
- [27] Yunhui Liu, Tieke He, Tao Zheng, and Jianhua Zhao. 2024. Negative-Free Self-Supervised Gaussian Embedding of Graphs. *Neural Networks* (2024).
- [28] Yixin Liu, Zhao Li, Shirui Pan, Chen Gong, Chuan Zhou, and George Karypis. 2021. Anomaly detection on attributed networks via contrastive self-supervised learning. *IEEE transactions on neural networks and learning systems* 33, 6 (2021), 2378–2392.
- [29] Yunhui Liu, Huaisong Zhang, Tieke He, Tao Zheng, and Jianhua Zhao. 2024. Bootstrap latents of nodes and neighbors for graph self-supervised learning. In *Joint European Conference on Machine Learning and Knowledge Discovery in Databases*. Springer, 76–92.
- [30] Zhining Liu, Ruizhong Qiu, Zichen Zeng, Hyunsik Yoo, David Zhou, Zhe Xu, Yada Zhu, Kommy Weldelemariam, Jingrui He, and Hanghang Tong. 2024. Class-Imbalanced Graph Learning without Class Rebalancing. In *Forty-first International Conference on Machine Learning*.
- [31] Sito Luan, Chenqing Hua, Qincheng Lu, Jiaqi Zhu, Mingde Zhao, Shuyuan Zhang, Xiao-Wen Chang, and Doina Precup. 2022. Revisiting heterophily for graph neural networks. *Advances in neural information processing systems* 35 (2022), 1362–1375.
- [32] Xiaoxiao Ma, Ruikun Li, Fanzhen Liu, Kaize Ding, Jian Yang, and Jia Wu. 2024. Graph anomaly detection with few labels: A data-centric approach. In *Proceedings of the 30th ACM SIGKDD Conference on Knowledge Discovery and Data Mining*. 2153–2164.
- [33] Yao Ma, Xiaorui Liu, Neil Shah, and Jiliang Tang. 2022. Is Homophily a Necessity for Graph Neural Networks?. In *International Conference on Learning Representations*.
- [34] Haitao Mao, Zhikai Chen, Wei Jin, Haoyu Han, Yao Ma, Tong Zhao, Neil Shah, and Jiliang Tang. 2023. Demystifying structural disparity in graph neural networks: Can one size fit all? *Advances in neural information processing systems* (2023).
- [35] Julian John McAuley and Jure Leskovec. 2013. From amateurs to connoisseurs: modeling the evolution of user expertise through online reviews. In *Proceedings of the 22nd international conference on World Wide Web*. 897–908.

- [36] Hongbin Pei, Bingzhe Wei, Kevin Chen-Chuan Chang, Yu Lei, and Bo Yang. 2020. Geom-GCN: Geometric Graph Convolutional Networks. In *International Conference on Learning Representations*.
- [37] Oleg Platonov, Denis Kuznedelev, Michael Diskin, Artem Babenko, and Liudmila Prokhorenkova. 2023. A critical look at the evaluation of GNNs under heterophily: Are we really making progress? In *The Eleventh International Conference on Learning Representations*.
- [38] Hezhe Qiao and Guansong Pang. 2023. Truncated affinity maximization: One-class homophily modeling for graph anomaly detection. *Advances in Neural Information Processing Systems* (2023).
- [39] Hezhe Qiao, Hanghang Tong, Bo An, Irwin King, Charu Aggarwal, and Guansong Pang. 2024. Deep graph anomaly detection: A survey and new perspectives. *arXiv preprint arXiv:2409.09957* (2024).
- [40] Hezhe Qiao, Qingsong Wen, Xiaoli Li, Ee-Peng Lim, and Guansong Pang. 2024. Generative Semi-supervised Graph Anomaly Detection. *Advances in neural information processing systems* (2024).
- [41] Shebuti Rayana and Leman Akoglu. 2015. Collective opinion spam detection: Bridging review networks and metadata. In *Proceedings of the 21th ACM SIGKDD international conference on knowledge discovery and data mining*. 985–994.
- [42] Jianheng Tang, Fengrui Hua, Ziqi Gao, Peilin Zhao, and Jia Li. 2023. GADBenchmark: Revisiting and benchmarking supervised graph anomaly detection. *Advances in Neural Information Processing Systems* 36 (2023), 29628–29653.
- [43] Jianheng Tang, Jiajin Li, Ziqi Gao, and Jia Li. 2022. Rethinking graph neural networks for anomaly detection. In *International Conference on Machine Learning*. PMLR, 21076–21089.
- [44] Shantanu Thakoor, Corentin Tallec, Mohammad Gheshlaghi Azar, Mehdi Azabou, Eva L Dyer, Remi Munos, Petar Veličković, and Michal Valko. 2022. Large-Scale Representation Learning on Graphs via Bootstrapping. In *International Conference on Learning Representations*.
- [45] Petar Veličković, Guillem Cucurull, Arantxa Casanova, Adriana Romero, Pietro Liò, and Yoshua Bengio. 2018. Graph Attention Networks. In *International Conference on Learning Representations*.
- [46] Petar Veličković, William Fedus, William L. Hamilton, Pietro Liò, Yoshua Bengio, and R Devon Hjelm. 2019. Deep Graph Infomax. In *International Conference on Learning Representations*.
- [47] Junfu Wang, Yuanfang Guo, Liang Yang, and Yunhong Wang. 2024. Understanding Heterophily for Graph Neural Networks. In *Forty-first International Conference on Machine Learning*.
- [48] Minjie Wang, Da Zheng, Zihao Ye, Quan Gan, Mufei Li, Xiang Song, Jinjing Zhou, Chao Ma, Lingfan Yu, Yu Gai, et al. 2019. Deep graph library: A graph-centric, highly-performant package for graph neural networks. *arXiv preprint arXiv:1909.01315* (2019).
- [49] Xiyuan Wang and Muhan Zhang. 2022. How powerful are spectral graph neural networks. In *International conference on machine learning*.
- [50] Yanling Wang, Jing Zhang, Shasha Guo, Hongzhi Yin, Cuiping Li, and Hong Chen. 2021. Decoupling representation learning and classification for gnn-based anomaly detection. In *Proceedings of the 44th international ACM SIGIR conference on research and development in information retrieval*. 1239–1248.
- [51] Mark Weber, Giacomo Domeniconi, Jie Chen, Daniel Karl I Weidele, Claudio Ballei, Tom Robinson, and Charles E Leiserson. 2019. Anti-money laundering in bitcoin: Experimenting with graph convolutional networks for financial forensics. *arXiv preprint arXiv:1908.02591* (2019).
- [52] Jiaying Wu and Bryan Hooi. 2023. Decor: Degree-corrected social graph refinement for fake news detection. In *Proceedings of the 29th ACM SIGKDD Conference on Knowledge Discovery and Data Mining*. 2582–2593.
- [53] Keyulu Xu, Weihua Hu, Jure Leskovec, and Stefanie Jegelka. 2019. How Powerful are Graph Neural Networks? In *International Conference on Learning Representations*.
- [54] Jure Zbontar, Li Jing, Ishan Misra, Yann LeCun, and Stéphane Deny. 2021. Barlow twins: Self-supervised learning via redundancy reduction. In *International conference on machine learning*.
- [55] Hengrui Zhang, Qitian Wu, Junchi Yan, David Wipf, and Philip S Yu. 2021. From canonical correlation analysis to self-supervised graph neural networks. *Advances in Neural Information Processing Systems* 34 (2021), 76–89.
- [56] Jiong Zhu, Yujun Yan, Lingxiao Zhao, Mark Heimann, Leman Akoglu, and Dana Koutra. 2020. Beyond homophily in graph neural networks: Current limitations and effective designs. *Advances in neural information processing systems* 33 (2020), 7793–7804.
- [57] Yanqiao Zhu, Yichen Xu, Feng Yu, Qiang Liu, Shu Wu, and Liang Wang. 2020. Deep graph contrastive representation learning. *arXiv preprint arXiv:2006.04131* (2020).
- [58] Yanqiao Zhu, Yichen Xu, Feng Yu, Qiang Liu, Shu Wu, and Liang Wang. 2021. Graph contrastive learning with adaptive augmentation. In *Proceedings of the web conference 2021*. 2069–2080.
- [59] Wei Zhuo, Zemin Liu, Bryan Hooi, Bingsheng He, Guang Tan, Rizal Fathony, and Jia Chen. 2024. Partitioning message passing for graph fraud detection. In *The Twelfth International Conference on Learning Representations*.

A Related Works

A.1 Graph Anomaly Detection

GNN-based approaches have emerged as a promising paradigm for GAD, due to their strong ability to capture both complex structural and node attribute patterns in graph data. A comprehensive and up-to-date survey of deep GAD methods is provided in [39], while BOND [24] and GADBenchmark [42] establish performance benchmarks for unsupervised and semi-/supervised GAD approaches, respectively.

Unsupervised GAD approaches do not rely on labeled data for training and instead use unsupervised learning techniques to identify anomaly patterns in graph data. For instance, DOMINANT [8] employs a graph autoencoder to reconstruct both attributes and structure using GNNs. CoLA [28] explores the consistency between anomalies and their neighbors across different contrastive views to assess node irregularity. VGOD [18] combines variance-based and attribute reconstruction models to detect anomalies in a balanced manner. TAM [38] introduces local affinity as an anomaly measure, aiming to learn tailored node representations for GAD by maximizing the local affinity between nodes and their neighbors.

Semi-/supervised GAD approaches assume that labels for some normal and abnormal nodes are available for training. They aim to assign labels by learning a decision boundary between normal and abnormal nodes. For example, BWGNN [43] uses a Beta graph wavelet to learn band-pass filters that capture anomaly signals. AM-Net [3] employs a restricted Bernstein polynomial parameterization to approximate filters in multi-frequency groups. CARE-GNN [9], PCGNN [25], and GHRN [10] adaptively prune inter-class edges based on neighbor distributions or the graph spectrum. PMP [59] introduces a partitioned message-passing mechanism to handle homophilic and heterophilic neighbors independently. To address settings with limited labeled data, CGenGA [32] proposes a diffusion-based graph generation method to synthesize additional training nodes, while ConsisGAD [5] incorporates learnable data augmentation to utilize the abundance of unlabeled data for consistency training. Furthermore, GGAD [40] introduces a novel semi-supervised framework using only labeled normal nodes.

Additionally, several works have explored GAD within the pre-training and fine-tuning paradigm. DCI [50] decouples representation learning and classification through a cluster-enhanced self-supervised learning task. [6] evaluates the performance of DGI [46] and GraphMAE [16] for GAD, demonstrating the potential of leveraging graph pre-training to enhance GAD with limited supervision. However, most existing methods pre-train a uniform global low-pass filter (e.g., GCN [21]) and then fine-tune a classifier on frozen node representations. The heterophily of abnormal nodes in GAD presents a significant challenge for directly applying these methods. To address this, we propose a pre-training and fine-tuning framework tailored for GAD, which incorporates both low-&high-pass filter pre-training and node-&dimension-adaptive fine-tuning.

A.2 Graph Pre-Training

Graph pre-training has emerged as a promising paradigm for label-efficient learning [19]. These methods first learn universal knowledge from unlabeled data using self-supervised objectives, which is then transferred to tackle specific downstream tasks. Existing

pre-training approaches can be broadly categorized into two groups: contrastive and non-contrastive approaches. Contrastive approaches typically follow the principle of mutual information maximization [15], where the objective functions contrast positive pairs against negative ones. For instance, DGI [46] and DCI [50] focus on representation learning by maximizing the mutual information between node-level representations and a global summary representation. GRACE [57], GCA [58], and NS4GC [26] learn node representations by pulling together the representations of the same node (positive pairs) across two augmented views, while pushing apart the representations of different nodes (negative pairs) across both views. Non-contrastive approaches, on the other hand, eliminate the need for negative samples. For example, CCA-SSG [55] and G-BT [2] aim to learn augmentation-invariant information while introducing feature decorrelation to capture orthogonal features. BGRL [44] and BLNN [29] employ asymmetric architectures that learn node representations by predicting alternative augmentations of the input graph and maximizing the similarity between the predictions and their corresponding targets. GraphMAE [16] focuses on feature reconstruction using a masking strategy and scaled cosine error. Additionally, SSGE [27] minimizes the distance between the distribution of learned representations and the isotropic Gaussian distribution to promote the uniformity of node representations. However, the methods discussed above rely on low-pass GNN encoders that inherently smooth neighbor representations, leading to unsatisfactory performance on heterophilic abnormal nodes. Although a recent work PolyGCL [4] employs both low- and high-pass encoders, it combines them using a simple linear strategy to obtain final node representations for fine-tuning. This approach is less flexible and effective than our proposed node- and dimension-adaptive fine-tuning strategy, as demonstrated in Theorem 1.

B Proofs

B.1 Proof of Proposition 1

PROOF. We first prove that the total spectral energy of $\alpha = U^\top \Delta y = (\alpha_1, \dots, \alpha_n)$ is constant with $\sum_{i=1}^n \alpha_i^2 = n$. Recall that L is symmetric and positive semi-definite, U^\top can be chosen to be an orthogonal matrix. Denote the element of the i -th row and j -th column of U^\top as u_{ij} .

$$\begin{aligned} \sum_{i=1}^n \alpha_i^2 &= \sum_{i=1}^n \left(\sum_{j=0}^n u_{ij} \Delta y_j \right)^2 \\ &= \sum_{i=1}^n \sum_{j=0}^n u_{ij}^2 + 2 \sum_{i=1}^n \left(\sum_{j=0}^n \sum_{k=0}^n u_{ij} u_{ik} \Delta y_j \Delta y_k \mathbf{1}\{j \neq k\} \right) \\ &= \sum_{i=1}^n \sum_{j=0}^n u_{ij}^2 + 2 \sum_{j=0}^n \sum_{k=0}^n \left(\Delta y_j \Delta y_k \sum_{i=1}^n u_{ij} u_{ik} \mathbf{1}\{j \neq k\} \right) \quad (14) \\ &= \sum_{i=1}^n \sum_{j=0}^n u_{ij}^2 \quad (\text{Orthogonality}) \\ &= n \end{aligned}$$

Then we prove that the spectral energy concentrates more on high frequencies with an increasing level of heterophily. Let the edge set consist of three disjoint subsets $\mathcal{E} = \mathcal{E}_{nn} \cup \mathcal{E}_{aa} \cup \mathcal{E}_{an}$. \mathcal{E}_{an}

denotes the set of inter-class edges while \mathcal{E}_{nn} and \mathcal{E}_{aa} represent the sets of intra-class edges for normal and abnormal nodes respectively. Thus, the edge homophily is reformulated as:

$$h = \frac{|\mathcal{E}_{nn}| + |\mathcal{E}_{aa}|}{|\mathcal{E}_{nn}| + |\mathcal{E}_{aa}| + |\mathcal{E}_{an}|} = \frac{|\mathcal{E}_{nn}| + |\mathcal{E}_{aa}|}{|\mathcal{E}|}, \quad (15)$$

subsequently, we have:

$$1 - h = \frac{|\mathcal{E}_{an}|}{|\mathcal{E}|} = \frac{\frac{1}{4} \sum_{e_{ij} \in \mathcal{E}} (y_i - y_j)^2}{\frac{1}{2} \sum_{i=1}^n D_{ii}} = \frac{\mathbf{y}^\top L \mathbf{y}}{2 \text{Tr}(L)}. \quad (16)$$

With $\alpha = U^\top \mathbf{y}$, we have $\mathbf{y}^\top L \mathbf{y} = \mathbf{y}^\top U \Lambda U^\top \mathbf{y} = \sum_{i=1}^n \alpha_i^2 \lambda_i$ and $\text{Tr}(L) = \text{Tr}(\Lambda U^\top U) = \sum_{i=1}^n \lambda_i$, leading to

$$\frac{\sum_{i=1}^n \alpha_i^2 \lambda_i}{\sum_{i=1}^n \lambda_i} = 2(1 - h), \quad (17)$$

which indicates that graphs with different homophily ratios respond to different frequencies. Specifically, since $\sum_{i=1}^n \alpha_i^2 = n$, the sum $\sum_{i=1}^n \alpha_i^2 \lambda_i$ is a convex combination of non-decreasing eigenvalues/frequencies λ_i , weighted by α_i^2 .

For a graph dataset where the heterophily of abnormal nodes is relatively low with $h \rightarrow 1$, the value of $\frac{\sum_{i=1}^n \alpha_i^2 \lambda_i}{\sum_{i=1}^n \lambda_i}$ approaches 0, implying that the spectral energy concentrates more on low-frequency components (i.e., larger α_i^2 is assigned to smaller eigenvalue λ_i). In contrast, when the heterophily of abnormal nodes increases, either the number of inter-class edges increases ($|\mathcal{E}_{an}| \uparrow$) or the intra-class edges within anomalies reduce ($|\mathcal{E}_{aa}| \downarrow$). According to Eq. (16), the homophily level h decreases and subsequently $\frac{\sum_{i=1}^n \alpha_i^2 \lambda_i}{\sum_{i=1}^n \lambda_i}$ moves further from 0, signifying that the spectral energy shifts toward higher-frequency components. \square

B.2 Proof of Proposition 2

PROOF. Given $\alpha = U^\top \Delta y = (\alpha_1, \dots, \alpha_n)$ and $\beta = U^\top X = (\beta_1, \dots, \beta_n)$, we adopt the assumption introduced in [4, 23] regarding their basic correlation.

ASSUMPTION 1. α and β are positively correlated in the spectral domain, that is, $\mathbb{E}(\alpha) = w\beta$, $w > 0$.

This assumption is consistent with the CSBM model [4], where a linear correlation exists between the node labels \mathbf{y} and the features X , which can be extended to the spectral domain by left multiplying U^\top . Then, the Spectral Regression Loss (SRL) between α and $g(\Lambda)\beta$ is:

$$\begin{aligned} \mathcal{L}(\mathcal{G}) &= \sum_{i=1}^n \left(\frac{\alpha_i}{\sqrt{n}} - \frac{g(\lambda_i)\beta_i}{\sqrt{\sum_{j=1}^n g(\lambda_j)^2 \beta_j^2}} \right)^2 \\ &= 2 - \frac{1}{T} \left(\sum_{i=1}^n \alpha_i^2 g(\lambda_i) \right). \end{aligned} \quad (18)$$

Here $T = \frac{\sqrt{n}}{2} \cdot \sqrt{\sum_{i=1}^n g(\lambda_i)^2 \alpha_i^2}$, which has the following upper bound:

$$T = \frac{\sqrt{n}}{2} \cdot \sqrt{\sum_{i=1}^n g(\lambda_i)^2 \alpha_i^2} \leq c\sqrt{n} \cdot \frac{\sqrt{n}}{2} = \frac{n}{2}, \quad (19)$$

where " \leq " follows from the bounded restriction $g(\lambda) \in [0, c]$. Consequently, there exists an upper bound for $\mathcal{L}(\mathcal{G})$:

$$\begin{aligned}\mathcal{L}(\mathcal{G}) &= 2 - \frac{1}{T} \left(\sum_{i=1}^n \alpha_i^2 g(\lambda_i) \right) \\ &\leq 2 - \frac{2}{cn} \left(\sum_{i=1}^n \alpha_i^2 g(\lambda_i) \right) \\ &= 2 - \mathcal{L}_t,\end{aligned}\quad (20)$$

where minimizing the upper bound of \mathcal{L} is equivalent to maximizing \mathcal{L}_t . Note that for $\mathcal{L}_t = \frac{2}{cn} (\sum_{i=1}^n \alpha_i^2 g(\lambda_i))$, ignoring the constant coefficient, it is essentially a convex combination of $g(\lambda_i)$, where $\sum_{i=1}^n \alpha_i^2 = n$.

For a homophilic graph, where $h \rightarrow 1$, Proposition 1 shows that the smaller eigenvalue λ_i is allocated more α_i^2 , implying that λ_i and α_i^2 exhibit opposite monotonicity (λ_i is non-decreasing while α_i^2 is non-increasing). In order to maximize \mathcal{L}_t (the convex combination of $g(\lambda_i)$), a larger value of $g(\lambda_i)$ should be assigned to larger α_i^2 . Thus, it is reasonable for the filter function $g(\cdot)$ to be a low-pass filter. In the context of GAD, the heterophily of abnormal nodes will lead to α concentrating more on high frequencies. As a result, the low-pass filter that maximizes \mathcal{L}_t when $h \rightarrow 1$ will not necessarily maximize, leading to a larger SRL $\mathcal{L}(\mathcal{G})$ and poorer performance.. In the extreme case where $h \rightarrow 0$, the larger eigenvalue λ_i is allocated more α_i^2 , meaning that α_i^2 also exhibits non-decreasing monotonicity. In this case, the filter function $g(\cdot)$ is expected to be a high-pass filter. \square

B.3 Proof of Theorem 1

PROOF. The proof is derived from [1], which analyzes the linear separability of a single graph convolution under a single CSBM model with only one pattern $CSBM(n, \mu, \nu, (p, q))$. We extend the analysis to our $ASBM(n_a, n_n, \mu, \nu, (p_1, q_1), (p_2, q_2), P_a, P_n)$.

Following [1], our analysis is based on the following assumptions: 1) The graph size n is relatively large, with $\omega(d \log d) \leq n \leq O(\text{poly}(d))$. 2) The graph is not too sparse, with $p_1, q_1, p_2, q_2 = \omega(\log^2(n)/n)$. The first assumption ensures that the number of nodes is at least quasilinearly large and at most polynomially large relative to the feature dimension. The second assumption ensures that the CSBM is not excessively sparse, maintaining a significant difference between the number of intra-class and inter-class edges. Additionally, we assume that the sizes of the homophilic and heterophilic node sets are approximately equal.

For simplicity, we use the random walk normalized adjacency matrix, $D^{-1}A$, as the low-pass filter, and its negative, $-D^{-1}A$, as the high-pass filter [1, 13, 31, 33, 34, 47]. Due to the Gaussian distribution of node features, the filtered node features also follow a Gaussian distribution. Specifically, for the low-pass filtered node features $\hat{X} = D^{-1}AX$, the means of nodes in different classes and

patterns are given by [1]:

$$\mathbb{E}(\hat{X}_i) = \begin{cases} \frac{p_1\mu + q_1\nu}{p_1 + q_1}(1 + o(1)) & \text{for } i \in C_a \cap \mathcal{H}_o, \\ \frac{q_1\mu + p_1\nu}{p_1 + q_1}(1 + o(1)) & \text{for } i \in C_n \cap \mathcal{H}_o, \\ \frac{p_2\mu + q_2\nu}{p_2 + q_2}(1 + o(1)) & \text{for } i \in C_a \cap \mathcal{H}_e, \\ \frac{q_2\mu + p_2\nu}{p_2 + q_2}(1 + o(1)) & \text{for } i \in C_n \cap \mathcal{H}_e, \end{cases} \quad (21)$$

where C_a and C_n represent the abnormal and normal node sets, respectively, while \mathcal{H}_o and \mathcal{H}_e denote the homophilic and heterophilic node sets. The covariance matrix for \hat{X}_i is given by $\mathbb{C}(\hat{X}_i) = \frac{1}{dn}D_{ii}$. Based on Lemma 2 in [1], for any unit vector w , we have

$$\left| \left(\hat{X}_i - \mathbb{E}(\hat{X}_i) \right) \cdot w \right| = O \left(\sqrt{\frac{\log n}{dn(p_1 + q_1)}} \right). \quad (22)$$

When considering only the nodes in the homophily set \mathcal{H}_o , Lemma 3 in [1] shows that an optimal linear classifier can be found with the following parameters:

$$w^* = R \frac{\nu - \mu}{\|\mu - \nu\|}, \quad b^* = -\frac{\langle \mu + \nu, w^* \rangle}{2}, \quad (23)$$

where R is the norm constraint, i.e., $\|w\| \leq R$, and the distance between μ and ν is sufficiently large, with $\|\mu - \nu\| = \Omega(\frac{\log n}{\sqrt{dn(p_1 + q_1)}})$. This linear classifier can correctly separate homophily nodes \mathcal{H}_o . Specifically, for $i \in C_a \cap \mathcal{H}_o$, we have:

$$\begin{aligned}\langle \hat{X}_i, w^* \rangle + b^* &= \frac{\langle p_1\mu + q_1\nu, w^* \rangle}{p_1 + q_1}(1 + o(1)) + O \left(\|w^*\| \sqrt{\frac{\log n}{dn(p_1 + q_1)}} \right) - \frac{\langle \mu + \nu, w^* \rangle}{2} \\ &= \frac{\langle 2p_1\mu + 2q_1\nu - (p_1 + q_1)(\mu + \nu), w^* \rangle}{2(p_1 + q_1)}(1 + o(1)) + o(\|w^*\|) \\ &= \frac{p_1 - q_1}{2(p_1 + q_1)} \langle \mu - \nu, w^* \rangle (1 + o(1)) + o(\|w^*\|) \\ &= -\frac{R(p_1 - q_1)}{2(p_1 + q_1)} \|\mu - \nu\| (1 + o(1)) < 0.\end{aligned}\quad (24)$$

Similarly, for $i \in C_n \cap \mathcal{H}_o$, we obtain:

$$\langle \hat{X}_i, w^* \rangle + b^* = -\frac{R(q_1 - p_1)}{2(p_1 + q_1)} \|\mu - \nu\| (1 + o(1)) > 0. \quad (25)$$

However, if we apply this linear classifier to the heterophilic node set \mathcal{H}_e , where $p_2 < q_2$, all nodes are misclassified:

$$\langle \hat{X}_i, w^* \rangle + b^* = \begin{cases} -\frac{R(p_2 - q_2)}{2(p_2 + q_2)} \|\mu - \nu\| (1 + o(1)) > 0 & \text{for } i \in C_a \cap \mathcal{H}_e, \\ -\frac{R(q_2 - p_2)}{2(p_2 + q_2)} \|\mu - \nu\| (1 + o(1)) < 0 & \text{for } i \in C_n \cap \mathcal{H}_e. \end{cases} \quad (26)$$

Next, consider the high-pass filtered node features $\hat{X} = -D^{-1}AX$, the mean of nodes in different classes and patterns are given by:

$$\mathbb{E}(\hat{X}_i) = \begin{cases} \frac{p_1\mu + q_1\nu}{p_1 + q_1}(1 + o(1)) & \text{for } i \in C_a \cap \mathcal{H}_o, \\ -\frac{q_1\mu + p_1\nu}{p_1 + q_1}(1 + o(1)) & \text{for } i \in C_n \cap \mathcal{H}_o, \\ -\frac{p_2\mu + q_2\nu}{p_2 + q_2}(1 + o(1)) & \text{for } i \in C_a \cap \mathcal{H}_e, \\ -\frac{q_2\mu + p_2\nu}{p_2 + q_2}(1 + o(1)) & \text{for } i \in C_n \cap \mathcal{H}_e. \end{cases} \quad (27)$$

Applying the same linear classifier with w^* and b^* yields the following results:

$$\langle \hat{X}_i, w^* \rangle + b^* = \begin{cases} \frac{R(p_2 - q_2)}{2(p_2 + q_2)} \|\mu - \nu\|(1 + o(1)) < 0 & \text{for } i \in C_a \cap \mathcal{H}_e, \\ \frac{R(q_2 - p_2)}{2(p_2 + q_2)} \|\mu - \nu\|(1 + o(1)) < 0 & \text{for } i \in C_n \cap \mathcal{H}_e. \end{cases} \quad (28)$$

Therefore, the same linear classifier is capable of separating both the homophilic node set \mathcal{H}_o and the heterophilic node set \mathcal{H}_e . And according to part 2 of Theorem 1 in [1], we have

$$\mathbb{P}\left(\left(\hat{X}_i\right)_{i \in \mathcal{V}^L} \text{ is linearly separable}\right) = 1 - o_d(1), \quad (29)$$

where $o_d(1)$ denotes a quantity that converges to 0 as $d \rightarrow \infty$.

□

C Other Pre-Training Instantiations

Here, we describe the process for pre-training low- and high-pass graph encoders, $f_l(\cdot)$ and $f_h(\cdot)$, using InfoNCE [12] and Barlow Twins [54]. They are adopted by previous graph pre-training methods GRACE [57] and G-BT [2], respectively. Both of them aim to learn node representations invariant to augmentation. We begin by presenting the overall framework of GRACE and G-BT.

C.1 Overview of GRACE and G-BT

GRACE and G-BT consist of three key components: 1) a random graph augmentation generator \mathcal{T} , 2) a graph encoder $f(\cdot)$, and 3) a self-supervised objective function.

C.1.1 Graph Augmentation. Graph augmentation generates diverse graph views, enabling the learning of representations robust to variance. Two commonly employed strategies for augmentation are feature masking and edge dropping, which aim to enhance node feature and graph topology information, respectively.

- **Feature Masking** randomly selects a portion of the node features' dimensions and masks their elements with zeros. Formally, it first samples a random vector $\tilde{m} \in \{0, 1\}^F$, where each dimension is drawn from a Bernoulli distribution with probability $1 - p_m$, i.e., $\tilde{m}_i \sim \mathcal{B}(1 - p_m)$, $\forall i$. Then, the masked node features \tilde{X} are computed by $\|\tilde{X}\|_i^N \ x_i \odot \tilde{m}$, where \odot denotes the Hadamard product and $\|\cdot\|$ represents the stack operation (i.e., concatenating a sequence of vectors along a new dimension).

- **Edge Dropping** randomly drops a certain fraction of edges from the original graph. Formally, since only existing edges are removed, it first samples a random masking matrix $\tilde{M} \in$

$\{0, 1\}^{N \times N}$, with entries drawn from a Bernoulli distribution $\tilde{M}_{i,j} \sim \mathcal{B}(1 - p_d)$ if $A_{i,j} = 1$ for the original graph, and $\tilde{M}_{i,j} = 0$ otherwise. Here, p_d represents the probability of each edge being dropped. The corrupted adjacency matrix can then be computed as $\tilde{A} = A \odot \tilde{M}$.

C.1.2 Training Process. During each training epoch, we first select two random augmentation functions, $t^1 \sim \mathcal{T}$ and $t^2 \sim \mathcal{T}$, where \mathcal{T} represents a set of all possible feature masking and edge-dropping operations. Next, we generate two distinct augmented views: $(\tilde{A}^1, \tilde{X}^1) = t^1(A, X)$ and $(\tilde{A}^2, \tilde{X}^2) = t^2(A, X)$, based on the selected functions. These augmented views are then passed through a shared encoder $f(\cdot)$ to extract the corresponding node representations: $Z^1 = f(\tilde{A}^1, \tilde{X}^1) \in \mathbb{R}^{n \times e}$ and $Z^2 = f(\tilde{A}^2, \tilde{X}^2) \in \mathbb{R}^{n \times e}$. Finally, a self-supervised objective function is computed on Z^1 and Z^2 to optimize the model parameters.

C.1.3 Objective Function. GRACE uses the InfoNCE [12] loss to maximize the mutual information between two augmented views. This encourages the representations of positive pairs (derived from the same node through data augmentation) to be similar, while pushing apart the representations of negative pairs (from different nodes):

$$\mathcal{L}_{nce}(Z^1, Z^2) = - \sum_{i=1}^n \log \frac{e^{z_i^1 \cdot z_i^2 / \tau}}{\sum_{j=1}^n e^{z_i^1 \cdot z_j^2 / \tau}}, \quad (30)$$

where z_i^1 and z_i^2 are the ℓ_2 -normalized representations of two views of node i , and τ is a temperature hyperparameter.

G-BT applies the Barlow Twins [54] loss to learn augmentation-invariant information while reducing redundancy in the learned representations:

$$\mathcal{L}_{bt}(Z^1, Z^2) = \underbrace{\sum_{i=1}^e (1 - C_{ii})^2 + \lambda}_{\text{invariance term}} \underbrace{\sum_{i=1}^e \sum_{j \neq i} C_{ij}^2}_{\text{redundancy reduction term}} \quad (31)$$

where λ is a positive constant that balances the importance of the two terms, and $C = \frac{1}{n} Z^1 Z^2$ is the cross-correlation matrix computed between the node representations of the two augmented views. Note that Z^1 and Z^2 are batch-normalized so that each representation channel follows a zero-mean, unit-variance distribution.

C.2 Integrate GRACE and BT into PAF

When integrating GRACE and BT into PAF, both the low- and high-pass graph encoders, $f_l(\cdot)$ and $f_h(\cdot)$, must be pre-trained. At each epoch, the two augmented views are passed through both encoders, yielding the following node representations: $Z_L^1 = f_l(\tilde{A}^1, \tilde{X}^1)$, $Z_L^2 = f_l(\tilde{A}^2, \tilde{X}^2)$, $Z_H^1 = f_h(\tilde{A}^1, \tilde{X}^1)$, $Z_H^2 = f_h(\tilde{A}^2, \tilde{X}^2)$. The pre-training loss based on InfoNCE is then defined as:

$$\mathcal{L}_{pt} = \mathcal{L}_{nce}(Z_L^1, Z_L^2) + \mathcal{L}_{nce}(Z_H^1, Z_H^2). \quad (32)$$

Similarly, the pre-training loss based on Barlow Twins is defined as:

$$\mathcal{L}_{pt} = \mathcal{L}_{bt}(Z_L^1, Z_L^2) + \mathcal{L}_{bt}(Z_H^1, Z_H^2). \quad (33)$$

D Formulations of Aggregation Methods

Here, we provide the mathematical formulations of the aggregation methods described in Section 5.4. These aggregation methods aim to generate overall node representations Z by combining low- and high-pass node representations $Z_L \in \mathbb{R}^{n \times e}$ and $Z_H \in \mathbb{R}^{n \times e}$.

- The "Low" method uses only the low-pass node representations, i.e., $Z = Z_L$.
- The "High" method uses only the high-pass node representations, i.e., $Z = Z_H$.
- The "Mean" method averages the low- and high-pass node representations, i.e., $Z = 0.5 \cdot (Z_L + Z_H)$.
- The "Concat" method concatenates the low- and high-pass node representations, i.e., $Z = [Z_L, Z_H]$.
- The "Scalar" method uses a learnable scalar parameter $\alpha \in [0, 1]$ to adaptively combine low- and high-pass node representations, i.e., $Z = \alpha \cdot Z_L + (1 - \alpha) \cdot Z_H$.
- The "Vector" method uses learnable vector parameters $\alpha \in [0, 1]^{1 \times e}$ to adaptively combine each dimension of low- and high-pass node representations, i.e., $Z = \alpha \odot Z_L + (1 - \alpha) \odot Z_H$.
- The "Atten." method [3] employs an attention mechanism to learn the weights $\alpha_L, \alpha_H \in [0, 1]^{n \times 1}$ for n nodes, such that $Z = \alpha_L \cdot Z_L + \alpha_H \cdot Z_H$. Specifically, for node i with $Z_i^L, Z_i^H \in \mathbb{R}^{1 \times e}$, the attention scores are computed as

$$\begin{aligned}\omega_i^L &= \mathbf{q}^\top \cdot \tanh \left(\mathbf{W}_Z^L Z_i^{L^\top} + \mathbf{W}_X^L X_i \right), \\ \omega_i^H &= \mathbf{q}^\top \cdot \tanh \left(\mathbf{W}_Z^H Z_i^{H^\top} + \mathbf{W}_X^H X_i \right),\end{aligned}\quad (34)$$

where $\mathbf{W}_Z^L, \mathbf{W}_Z^H \in \mathbb{R}^{e' \times e}$ and $\mathbf{W}_X^L, \mathbf{W}_X^H \in \mathbb{R}^{e' \times d}$ are learnable parameter matrices, and $\mathbf{q} \in \mathbb{R}^{e' \times 1}$ is the shared attention vector. The final attention weights of node i are obtained by normalizing the attention values using the softmax function:

$$\begin{aligned}\alpha_i^L &= \frac{\exp(\omega_i^L)}{\exp(\omega_i^L) + \exp(\omega_i^H)}, \\ \alpha_i^H &= \frac{\exp(\omega_i^H)}{\exp(\omega_i^L) + \exp(\omega_i^H)}.\end{aligned}\quad (35)$$

E Additional Experimental Details

E.1 Datasets

Following GADBench [42], we conduct experiments on 10 real-world datasets spanning various scales and domains. Reddit [22], Weibo [22], Questions [37], and T-Social [43] focus on detecting anomalous accounts on social media platforms. Tolokers [37], Amazon [35], and YelpChi [41] are designed to identify fraudulent workers, reviews, and reviewers in crowdsourcing or e-commerce platforms. T-Finance [43], Elliptic [51], and DGraph-Fin [17] target the detection of fraudulent users, illicit entities, and overdue loans in financial networks. Dataset Statistics are presented in Table 3. Detailed descriptions of these datasets are as follows.

- **Reddit** [22]: This dataset includes a user-subreddit graph, capturing one month's worth of posts shared across various subreddits. It includes verified labels for banned users and focuses on the 1,000 most active subreddits and the 10,000

most engaged users, resulting in 672,447 interactions. Posts are represented as feature vectors based on Linguistic Inquiry and Word Count (LIWC) categories.

- **Weibo** [22]: This dataset consists of a user-hashtag graph from the Tencent-Weibo platform, containing 8,405 users and 61,964 hashtags. Suspicious activities are defined as posting two messages within a specific time frame, such as 60 seconds. Users engaged in at least five such activities are labeled as "suspicious," while others are categorized as "benign." The feature vectors are based on the location of posts and bag-of-words features.
- **Amazon** [35]: This dataset focuses on detecting users who are paid to write fake reviews for products in the Musical Instrument category on Amazon.com. It contains three types of relationships: U-P-U (users reviewing the same product), U-S-U (users giving the same star rating within one week), and U-V-U (users with top 5% mutual review similarities).
- **YelpChi** [41]: This dataset aims to identify anomalous reviews on Yelp.com that unfairly promote or demote products or businesses. It includes three types of edges: R-U-R (reviews by the same user), R-S-R (reviews for the same product with the same star rating), and R-T-R (reviews for the same product within the same month).
- **T-Finance** [43]: This dataset is designed to detect anomalous accounts in transaction networks. The nodes represent unique anonymized accounts with 10-dimensional features related to registration days, login activities, and interaction frequency. Edges represent transactions between accounts, and anomalies are annotated by human experts based on categories such as fraud, money laundering, and online gambling.
- **Elliptic** [51]: This dataset includes over 200,000 Bitcoin transactions (nodes), 234,000 directed payment flows (edges), and 166 node features. It maps Bitcoin transactions to real-world entities, categorizing them as either licit (e.g., exchanges, wallet providers, miners) or illicit (e.g., scams, malware, terrorist organizations, ransomware, and Ponzi schemes).
- **Tolokers** [37]: This dataset is derived from the Toloka crowdsourcing platform. Nodes represent workers who have participated in at least one of 13 selected projects. An edge connects two workers if they collaborated on the same task. The goal is to predict which workers were banned in any of the projects. Node features are based on worker profiles and task performance.
- **Questions** [37]: This dataset is collected from the Yandex Q question-answering platform. It includes users as nodes, with edges representing answers between users during a one-year period (September 2021 to August 2022). It focuses on users interested in the "medicine" topic. The task is to predict which users remained active by the end of the period. Node features include the mean of FastText embeddings for words in the user descriptions, with a binary feature indicating users without descriptions.

Table 3: Dataset statistics including the number of nodes and edges, the node feature dimension, the ratio of anomalies, the homophily ratio, the concept of relations, and the type of node features. h , h^a , and h^n represent the edge homophily, the average homophily for abnormal nodes, and the average homophily for normal nodes, respectively. As we can see, h^a is much smaller than h^n , indicating that abnormal nodes exhibit significantly higher heterophily compared to normal nodes. "Misc." refers to node features that are a combination of heterogeneous attributes, which may include categorical, numerical, and temporal information.

Dataset	#Nodes	#Edges	#Feat.	Anomaly	h	h^a	h^n	Relation Concept	Feature Type
Reddit	10,984	168,016	64	3.3%	0.947	0.000	0.994	Under Same Post	Text Embedding
Weibo	8,405	407,963	400	10.3%	0.977	0.858	0.977	Under Same Hashtag	Text Embedding
Amazon	11,944	4,398,392	25	9.5%	0.954	0.102	0.968	Review Correlation	Misc. Information
YelpChi	45,954	3,846,979	32	14.5%	0.773	0.195	0.867	Reviewer Interaction	Misc. Information
T-Finance	39,357	21,222,543	10	4.6%	0.971	0.543	0.976	Transaction Record	Misc. Information
Elliptic	203,769	234,355	166	9.8%	0.970	0.234	0.985	Payment Flow	Misc. Information
Tolokers	11,758	519,000	10	21.8%	0.595	0.476	0.679	Work Collaboration	Misc. Information
Questions	48,921	153,540	301	3.0%	0.840	0.111	0.922	Question Answering	Text Embedding
DGraph-Fin	3,700,550	4,300,999	17	1.3%	0.993	0.013	0.997	Loan Guarantor	Misc. Information
T-Social	5,781,065	73,105,508	10	3.0%	0.624	0.174	0.900	Social Friendship	Misc. Information

- **DGraph-Fin** [17]: This dataset is a large-scale dynamic graph from the Finvolution Group representing a financial industry social network. Nodes represent users, and edges indicate emergency contact relationships. Anomalous nodes correspond to users exhibiting overdue behaviors. The dataset includes over 3 million nodes, 4 million dynamic edges, and more than 1 million unbalanced ground-truth anomalies.
- **T-Social** [43]: This dataset targets anomalous accounts in social networks. Nodes share the same annotations and features as those in T-Finance, with edges representing friend relationships maintained for more than three months. Anomalous nodes are annotated by experts in categories like fraud, money laundering, and online gambling.

E.2 Baselines

We compare our model with a series of baseline methods, which can be categorized into the following groups: Standard GNN Architectures, including GCN [21], GIN [53], GAT [45]; GNNs Specialized for GAD, including PCGNN [25], BernNet [14], AMNet [3], BWGNN [43], GHRN [10], and ConsisGAD [5]; Graph Pre-Training Methods, including DGI [46], GRACE [57], DCI [50], BGRL [44], GraphMAE [16], G-BT [2], SSGE [27], and PolyGCL [4]. Detailed descriptions of these baselines are as follows.

E.2.1 Standard GNN Architectures.

- **GCN** [21] employs a convolutional operation on the graph to propagate information from each node to its neighboring nodes, enabling the network to learn a representation for each node based on its local neighborhood.
- **GIN** [53] is designed to capture the structural properties of a graph while preserving graph isomorphism. Specifically, it generates identical embeddings for graphs that are structurally identical, regardless of permutations in node labels.

- **GAT** [45] incorporates an attention mechanism, assigning different levels of importance to nodes during the information aggregation process. This allows the model to focus on the most relevant nodes within a neighborhood.

E.2.2 GNNs Specialized for GAD.

- **PCGNN** [25] uses a label-balanced sampler to select nodes and edges for training, ensuring a balanced label distribution in the induced subgraph. Additionally, it employs a learnable, parameterized distance function to select neighbors, filtering out redundant links while adding beneficial ones for improved fraud prediction.
- **BernNet** [14] provides a robust framework for designing and learning arbitrary graph spectral filters. It uses an order-K Bernstein polynomial approximation to estimate filters over the normalized Laplacian spectrum of a graph.
- **AMNet** [3] captures both low- and high-frequency signals by stacking multiple BernNets, adaptively combining signals from different frequency ranges.
- **BWGNN** [43] addresses the "right-shift" phenomenon in graph anomalies, where spectral energy distribution shifts from low to high frequencies. It uses a Beta kernel to address high-frequency anomalies through flexible, spatially- and spectrally-localized band-pass filters.
- **GHRN** [10] targets the heterophily problem in the spectral domain for graph anomaly detection. This method prunes inter-class edges to highlight and delineate the graph's high-frequency components.
- **ConsisGAD** [5] focuses on graph anomaly detection with limited supervision. It incorporates learnable data augmentation to utilize the abundance of unlabeled data for consistency training.

E.2.3 Graph Pre-Training Methods.

- **DGI** [46] learns representations by maximizing the mutual information between node representations and a global summary representation.
- **GRACE** [46] learns node representations by pulling together the representations of the same node (positive pairs) across two augmented views, while pushing apart the representations of different nodes (negative pairs) across both views.
- **DCI** [50] reduces inconsistencies between node behavior patterns and label semantics, and captures intrinsic graph properties within concentrated feature spaces by clustering the graph into multiple segments.
- **GraphMAE** [16] is a masked graph auto-encoder that focuses on feature reconstruction using both a masking strategy and scaled cosine error.
- **BGRL** [44] employs asymmetric architectures to learn node representations by predicting alternative augmentations of the input graph and maximizing the similarity between these predictions and their corresponding targets.
- **G-BT** [2] utilizes a cross-correlation-based loss function to reduce redundancy in the learned representations, which enjoys fewer hyperparameters and significantly reduced computation time.
- **SSGE** [27] minimizes the distance between the distribution of learned representations and an isotropic Gaussian distribution, promoting the uniformity of node representations.

- **PolyGCL** [4] addresses heterophilic challenges in graph pre-training by using polynomial filters as encoders and incorporating a combined linear objective between low- and high-frequency components in the spectral domain.

E.2.4 Implementation Details. We use the implementations of all baseline methods provided by GADBench [42] or the respective authors. Our PAF model is implemented using PyTorch and the Deep Graph Library (DGL) [48]. Experiments are conducted on a Linux server equipped with an Intel(R) Xeon(R) Gold 6248 CPU @ 2.50GHz and a 32GB NVIDIA Tesla V100 GPU. During the pre-training phase, each model is trained for up to 800 epochs using the Adam optimizer [20], with a patience of 20. Hyperparameters are tuned as follows: model depth $\in \{1, 2, 3\}$, learning rate $\in \{0.01, 0.001, 0.0001\}$, representation dimension $\in \{32, 64, 128, 256, 512\}$, activation function $\in \{\text{ReLU}, \text{ELU}, \text{PReLU}, \text{Tanh}\}$, and normalization $\in \{\text{none}, \text{batch}, \text{layer}\}$. For G-BT+PAF, the trade-off parameter λ in Eq. (31) is selected from $\{0.01, 0.005, 0.0001\}$. For GRACE+PAF, the temperature parameter τ in Eq. (30) is set to 0.9 by default. The feature masking ratio and edge dropping ratio are chosen from $\{0.0, 0.1, 0.2, 0.3, 0.4, 0.5\}$. During the fine-tuning phase, the classifier is trained for up to 500 epochs using the Adam optimizer [20], with a learning rate of 0.01 and weight decay selected from $\{0.0, 0.01, 0.0001\}$. The classifier with the highest validation AUROC score is selected for testing. The hyperparameters p_n and p_a are varied within the range of 0.0 to 1.0. All implementation code, pre-trained checkpoints, and specific hyperparameters are available at <https://anonymous.4open.science/r/PAF-163E>.

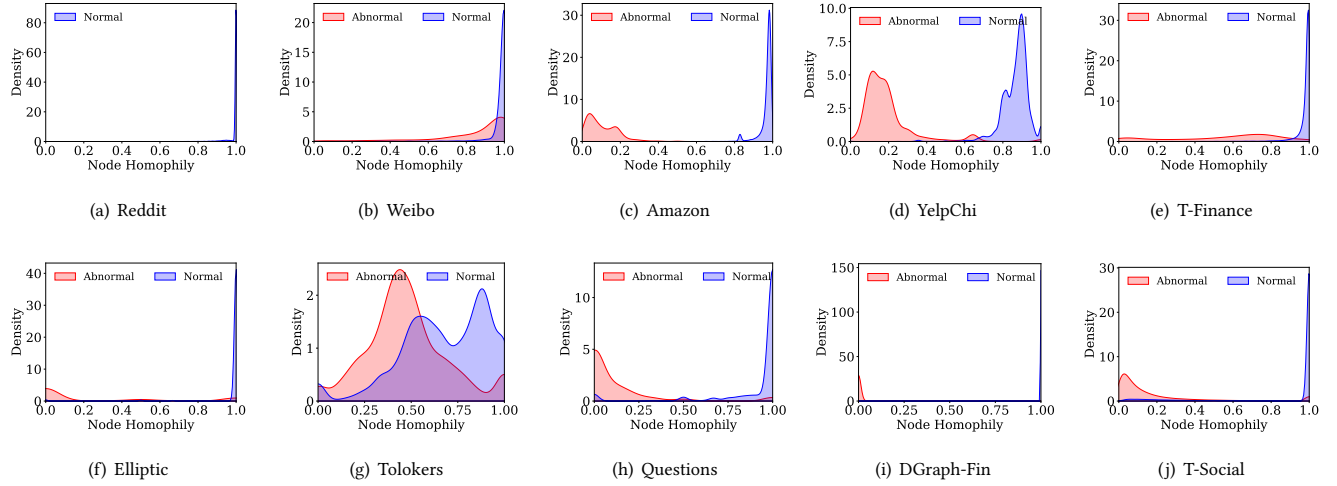


Figure 7: Distribution of node homophily across different datasets. GAD graphs display a mixed homophily-heterophily pattern: 1) Different nodes exhibit varying degrees of homophily/heterophily, and 2) Abnormal nodes tend to show higher heterophily than normal nodes. (On Reddit, we only plot the homophily distribution for normal nodes, since the node homophily of all abnormal nodes is 0.)

Table 4: Comparison of AUPRC for each model. “-” denotes “out of memory”.

Model	Reddit	Weibo	Amazon	Yelp.	T-Fin.	Ellip.	Tolo.	Quest.	DGraph.	T-Social
GCN	4.2±0.8	86.0±6.7	32.8±1.2	16.4±2.6	60.5±10.8	43.1±4.6	33.0±3.6	6.1±0.9	2.3±0.2	8.4±3.8
GIN	4.3±0.6	67.6±7.4	75.4±4.3	23.7±5.4	44.8±7.1	40.1±3.2	31.8±3.2	6.7±1.1	2.0±0.1	6.2±1.7
GAT	4.7±0.7	73.3±7.3	81.6±1.7	25.0±2.9	28.9±8.6	44.2±6.6	33.0±2.0	7.3±1.2	2.2±0.2	9.2±2.0
PCGNN	3.4±0.5	69.3±9.7	81.9±1.9	25.0±3.5	58.1±11.3	40.3±6.6	33.9±1.7	6.4±1.8	2.4±0.4	8.0±1.6
BernNet	4.9±0.3	66.6±5.5	81.2±2.4	23.9±2.7	51.8±12.4	40.0±4.1	28.9±3.5	6.7±2.1	2.5±0.2	4.2±1.2
AMNet	4.9±0.4	67.1±5.1	82.4±2.2	23.9±3.5	60.2±8.2	33.3±4.8	28.6±1.5	7.4±1.4	2.2±0.3	3.1±0.3
BWGNN	4.2±0.7	80.6±4.7	81.7±2.2	23.7±2.9	60.9±13.8	43.4±5.5	35.3±2.2	6.5±1.7	2.1±0.3	15.9±6.2
GHRN	4.2±0.6	77.0±6.2	80.7±1.7	23.8±2.8	63.4±10.4	44.2±5.7	35.9±2.0	6.5±1.7	2.3±0.3	16.2±4.6
ConsisGAD	4.5±0.5	64.6±5.5	78.7±5.7	25.9±2.9	79.7±4.7	47.8±8.2	33.7±2.7	7.9±2.4	2.0±0.2	41.3±5.0
DCI	4.3±0.4	76.2±4.3	72.5±7.9	24.0±4.8	51.0±7.2	43.4±4.9	32.1±4.2	6.1±1.3	2.0±0.2	7.4±2.5
GraphMAE	4.3±0.1	91.4±2.6	39.4±0.3	17.3±0.1	70.8±4.7	32.7±3.8	36.0±2.1	5.9±0.5	2.1±0.1	42.6±10.5
BGRL	5.3±0.3	<u>93.6±1.9</u>	43.9±4.6	19.2±1.6	61.7±5.1	47.4±6.0	38.3±3.3	8.4±2.0	2.0±0.2	46.7±8.4
SSGE	4.8±0.9	87.7±2.6	39.1±2.4	18.8±1.6	77.6±0.9	47.4±3.0	38.2±2.8	8.1±1.1	2.5±0.3	46.4±3.9
PolyGCL	5.2±0.8	87.3±2.1	79.7±6.6	24.3±2.5	43.3±6.4	50.0±5.2	33.0±1.8	5.7±0.8	2.2±0.3	40.6±7.0
DGI	4.8±0.6	90.8±2.5	46.5±3.7	17.0±1.2	75.0±4.9	45.9±2.5	39.7±0.8	6.4±1.2	2.1±0.2	37.8±6.1
+PAF	5.3±0.6	93.9±1.1	82.8±3.0	27.1±1.6	82.5±2.3	59.4±4.7	40.4±2.0	12.2±1.3	2.9±0.0	77.6±4.6
Avg.↑ +11.8	+0.5	+3.1	+36.3	+10.1	+7.5	+13.5	+0.7	+5.8	+0.8	+39.8
G-BT	5.0±0.7	87.5±3.9	38.7±2.2	18.8±1.6	76.8±1.8	45.2±4.4	37.9±2.8	<u>9.1±1.9</u>	<u>2.6±0.3</u>	42.2±7.4
+PAF	5.7±1.0	89.0±3.0	81.6±3.1	28.4±1.4	81.2±2.2	62.1±5.7	39.0±2.5	9.1±1.2	2.9±0.2	75.6±5.9
Avg.↑ +11.1	+0.7	+1.5	+42.9	+9.6	+4.4	+16.9	+1.1	+0.0	+0.3	+33.4
GRACE	4.7±0.3	90.8±1.8	51.3±4.3	18.2±1.6	79.3±0.7	48.1±3.6	37.4±2.8	8.9±1.7	-	-
+PAF	6.0±1.0	91.8±1.7	83.7±1.4	27.4±2.5	81.6±1.4	67.7±3.4	39.8±2.7	9.1±1.9	-	-
Avg.↑ +8.6	+1.3	+1.0	+32.4	+9.2	+2.3	+19.6	+2.4	+0.2	-	-

Table 5: Comparison of Rec@K for each model. “-” denotes “out of memory”.

Model	Reddit	Weibo	Amazon	Yelp.	T-Fin.	Ellip.	Tolo.	Quest.	DGraph.	T-Social
GCN	6.2±2.2	79.2±4.3	36.9±2.6	16.9±3.0	60.6±7.6	49.7±4.2	33.4±3.5	9.8±1.2	3.6±0.4	10.2±8.1
GIN	4.8±1.9	66.5±7.3	70.4±5.7	26.5±6.1	54.4±5.0	47.6±3.1	33.6±3.0	10.3±1.1	2.1±0.5	5.3±2.9
GAT	6.5±2.3	70.2±4.6	77.1±1.7	28.1±3.4	36.2±10.3	51.4±5.8	35.1±1.8	10.9±0.9	3.1±0.7	11.6±3.0
PCGNN	3.0±2.1	65.1±6.6	78.0±1.5	27.8±3.8	63.9±6.3	46.5±7.3	34.3±1.6	10.1±3.9	3.7±1.0	13.5±3.1
BernNet	6.4±1.5	60.9±4.6	77.2±2.1	26.8±3.1	60.5±11.1	47.0±4.5	30.1±3.8	10.3±2.7	3.8±0.6	3.3±2.8
AMNet	6.8±1.5	62.1±4.4	77.8±2.3	26.6±4.3	65.7±6.3	37.8±6.7	30.5±1.9	12.7±2.6	2.6±0.8	1.6±0.5
BWGNN	6.0±1.4	75.1±3.5	77.7±1.6	26.4±3.2	64.9±11.7	49.7±6.1	35.5±3.1	10.9±3.2	3.1±0.8	24.3±7.4
GHRN	6.3±1.5	72.4±2.6	77.7±1.3	26.9±3.1	67.7±4.3	50.8±4.8	36.1±3.1	11.1±3.4	3.4±0.7	24.6±7.0
ConsisGAD	6.3±2.5	58.6±4.6	77.5±2.8	28.7±3.2	76.5±4.2	50.8±7.8	34.8±2.3	12.8±3.1	1.8±0.5	48.5±4.6
DCI	4.5±1.4	68.5±3.5	68.3±7.2	26.8±5.3	58.5±6.3	50.0±3.8	33.5±5.6	9.9±1.9	2.3±0.7	6.3±6.8
GraphMAE	4.7±0.5	86.8±2.4	47.6±1.1	20.2±0.2	67.4±4.7	37.9±3.6	37.1±2.0	9.6±2.1	3.5±0.4	44.8±10.6
BGRL	7.4±1.1	90.3±1.1	45.3±3.7	21.6±1.5	59.2±3.4	51.0±4.7	38.2±3.1	11.5±3.6	2.7±0.6	47.1±5.2
SSGE	6.4±2.2	81.0±2.2	45.1±3.9	20.6±1.8	74.7±0.9	51.6±2.8	38.3±2.7	11.4±1.6	3.6±0.8	49.5±3.2
PolyGCL	7.4±2.5	81.7±2.9	72.5±7.5	27.5±2.9	50.4±3.8	55.0±2.5	35.6±1.8	9.0±2.4	1.9±0.7	44.7±5.1
DKI	6.5±1.3	85.5±2.1	49.2±2.2	18.8±1.2	71.7±4.8	48.0±2.1	39.1±1.1	9.8±2.8	3.1±0.7	43.2±4.3
+PAF	7.2±1.5	88.5±2.5	75.2±4.4	30.4±1.6	78.9±1.7	62.1±2.3	40.6±1.5	16.5±0.8	4.0±0.1	73.9±4.4
Avg.↑ +10.2	+0.7	+3.0	+26.0	+11.6	+7.2	+14.1	+1.5	+6.7	+0.9	+30.7
G-BT	6.8±1.7	85.1±3.6	46.3±3.4	20.6±1.5	74.0±1.9	50.7±3.7	38.3±2.8	12.0±3.4	3.8±0.6	46.2±6.0
+PAF	7.5±2.5	84.2±2.7	75.2±4.7	31.6±1.6	77.8±2.6	61.6±3.9	40.1±2.2	14.4±1.3	4.2±0.5	73.1±6.0
Avg.↑ +8.6	+0.7	-0.9	+28.9	+11.0	+3.8	+10.9	+1.8	+2.4	+0.4	+26.9
GRACE	5.6±2.6	85.6±2.5	51.8±4.5	20.4±1.4	74.8±1.1	52.4±3.7	38.4±2.0	13.0±1.9	-	-
+PAF	9.1±1.6	86.1±1.7	78.6±1.1	29.8±2.8	76.9±1.6	62.1±2.1	40.8±1.8	14.1±2.4	-	-
Avg.↑ +6.9	+3.5	+0.5	+26.8	+9.4	+2.1	+9.7	+2.4	+1.1	-	-

Table 6: Ablation study on each component of our PAF. The backbone is G-BT+PAF.

Variants			YelpChi			Elliptic			Questions			DGraph-Fin			
Z_L	Z_H	\mathcal{L}_{reg}	Aggr.	AUROC	AUPRC	Rec@K	AUROC	AUPRC	Rec@K	AUROC	AUPRC	Rec@K	AUROC	AUPRC	Rec@K
✓	✓	✓	NDApt	68.2±2.3	28.4±1.4	31.6±1.6	91.5±1.1	62.1±5.7	61.6±3.9	69.8±1.5	9.1±1.2	14.4±1.3	72.5±0.9	2.9±0.2	4.2±0.5
✓	✓	✗	NDApt	67.4±2.3	27.5±1.6	30.6±1.9	91.1±1.0	61.9±4.6	61.0±2.7	68.6±1.7	7.3±1.3	11.3±3.0	72.0±0.6	2.8±0.1	3.9±0.4
✓	✓	✗	Mean	67.6±2.3	27.7±1.7	30.6±1.9	90.8±1.0	60.4±5.6	60.5±3.7	68.6±1.5	7.3±1.1	11.4±2.7	71.9±0.7	2.8±0.1	3.9±0.3
✓	✓	✗	Concat	67.3±2.2	27.3±1.9	30.4±2.1	91.1±1.2	62.8±5.6	61.0±3.8	68.3±1.4	7.3±1.2	11.7±2.6	71.7±1.6	2.8±0.2	4.0±0.7
✓	✓	✗	Scalar	67.3±2.3	27.4±1.7	30.4±2.1	90.6±1.3	59.5±6.0	59.7±4.3	68.5±1.6	7.3±1.1	11.2±2.9	71.8±0.8	2.8±0.1	3.9±0.3
✓	✓	✗	Vector	67.5±2.4	27.6±1.7	30.5±1.9	90.7±1.3	60.2±6.7	60.2±4.6	68.6±1.5	7.3±1.1	11.3±2.8	71.9±0.7	2.8±0.1	3.9±0.3
✓	✓	✗	Atten.	63.6±1.9	24.1±1.6	27.3±1.7	88.7±2.1	53.9±6.9	59.6±5.7	68.2±1.8	7.1±1.0	11.2±2.8	72.0±0.6	2.8±0.1	4.0±0.3
✓	✗	✗	Low	56.5±1.3	18.7±1.2	21.1±1.4	88.9±1.1	50.2±3.4	52.0±3.2	69.6±0.9	9.0±1.1	14.3±1.2	70.4±1.3	2.7±0.2	4.1±0.4
✗	✓	✗	High	64.0±2.5	24.4±2.4	27.2±2.5	82.7±1.5	42.3±4.7	47.0±3.5	63.9±2.1	4.9±0.3	6.4±1.3	69.2±0.5	2.4±0.1	3.0±0.6

Table 7: Ablation study on each component of our PAF. The backbone is GRACE+PAF.

Variants			YelpChi			Elliptic			Questions			T-Finance			
Z_L	Z_H	\mathcal{L}_{reg}	Aggr.	AUROC	AUPRC	Rec@K	AUROC	AUPRC	Rec@K	AUROC	AUPRC	Rec@K	AUROC	AUPRC	Rec@K
✓	✓	✓	NDApt	66.2±3.2	27.4±2.5	29.8±2.8	90.7±1.2	67.7±3.4	62.1±2.1	69.0±4.4	9.1±1.9	14.1±2.4	94.3±0.4	81.6±1.4	76.9±1.6
✓	✓	✗	NDApt	65.7±2.7	27.2±2.1	29.3±2.3	90.6±1.1	67.1±3.9	61.8±2.3	68.7±3.5	8.6±1.7	13.5±2.4	94.2±0.6	81.3±2.1	76.1±2.0
✓	✓	✗	Mean	65.3±2.9	26.9±2.1	28.9±2.6	90.6±1.3	66.9±3.8	61.5±2.2	65.8±3.1	6.9±1.1	11.5±1.8	94.0±0.7	80.6±2.0	75.3±1.9
✓	✓	✗	Concat	65.0±3.2	26.7±2.6	29.1±2.9	90.5±1.4	68.2±3.5	62.4±2.9	65.5±3.7	6.9±1.1	11.8±1.8	93.4±1.2	79.5±3.0	74.2±3.2
✓	✓	✗	Scalar	66.0±2.9	27.5±2.4	29.4±2.5	90.4±1.2	66.8±3.6	61.6±2.6	64.2±3.8	6.2±1.0	10.3±2.3	94.1±0.6	81.2±1.5	76.1±1.6
✓	✓	✗	Vector	65.2±2.9	26.8±2.1	28.9±2.6	90.3±1.3	66.3±4.1	61.2±2.6	65.7±3.1	6.8±1.1	11.3±1.9	94.1±0.6	80.8±1.8	75.6±1.7
✓	✓	✗	Atten.	63.6±3.1	25.1±2.4	27.1±2.9	88.7±1.2	62.1±5.2	60.1±3.8	64.7±3.0	6.4±1.1	10.9±2.2	91.7±2.5	66.3±11.7	66.6±8.8
✓	✗	✗	Low	54.2±2.3	18.3±1.8	20.1±2.0	88.8±1.4	50.6±2.3	53.2±3.8	69.0±2.2	8.1±0.9	12.6±1.0	92.6±1.2	78.5±1.3	74.6±1.2
✗	✓	✗	High	64.0±3.0	25.2±2.4	27.4±2.4	83.6±2.1	49.7±3.8	50.8±3.3	60.3±4.0	5.3±0.8	9.0±2.0	80.6±2.3	23.8±5.0	32.5±7.0

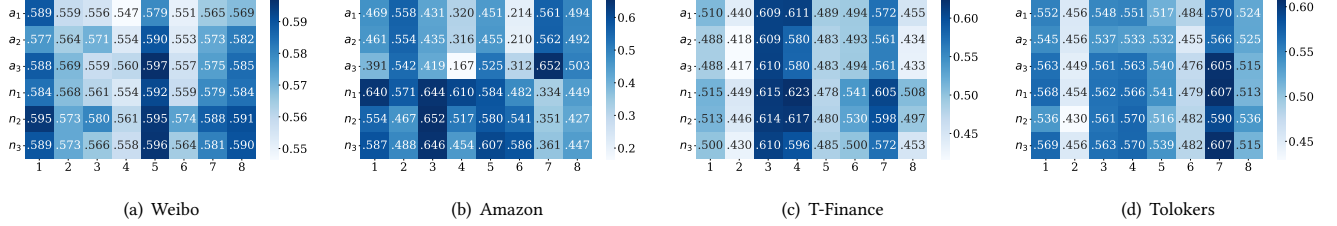


Figure 8: Visualization of the learned coefficients by the G-BT+PAF model for the top 8 dimensions. The nodes a_1, a_2, a_3 are 3 randomly selected abnormal nodes, while n_1, n_2, n_3 are 3 randomly selected normal nodes.

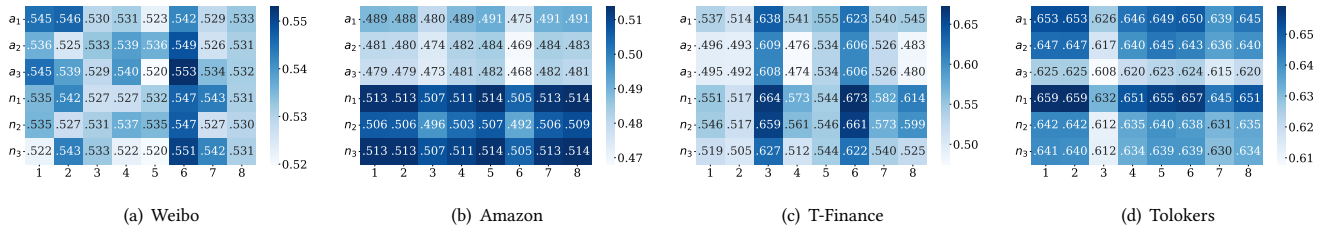


Figure 9: Visualization of the learned coefficients by the GRACE+PAF model for the top 8 dimensions. The nodes a_1, a_2, a_3 are 3 randomly selected abnormal nodes, while n_1, n_2, n_3 are 3 randomly selected normal nodes.

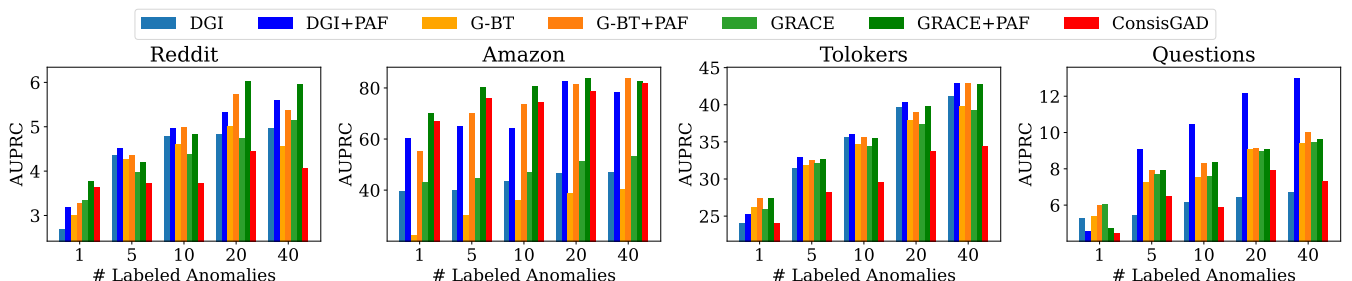


Figure 10: How the AUPRC score varies with different numbers of labeled anomalies.

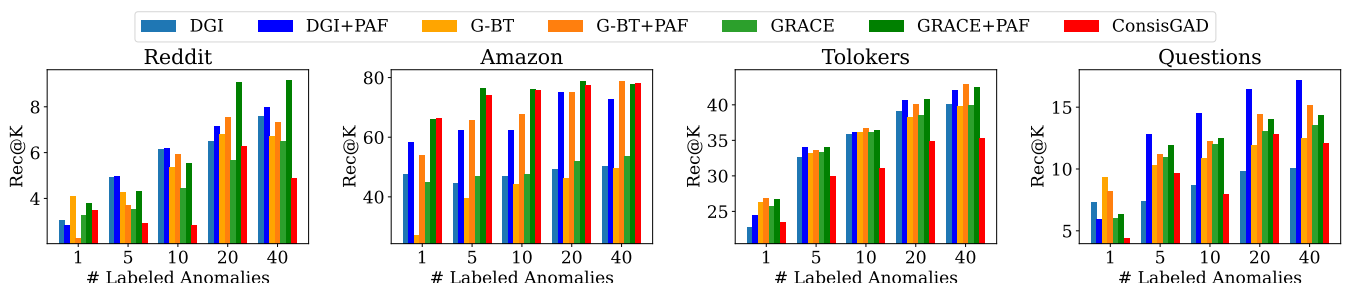


Figure 11: How the Rec@K score varies with different numbers of labeled anomalies.

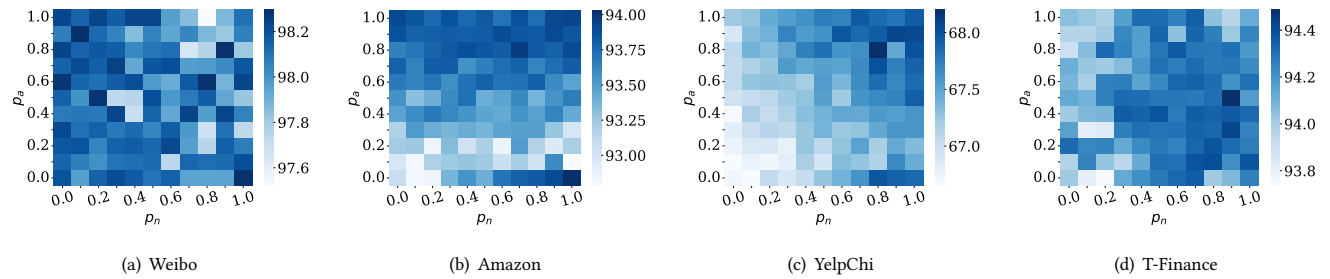


Figure 12: How the AUROC score of G-BT+PAF varies with different values of p_a and p_n .

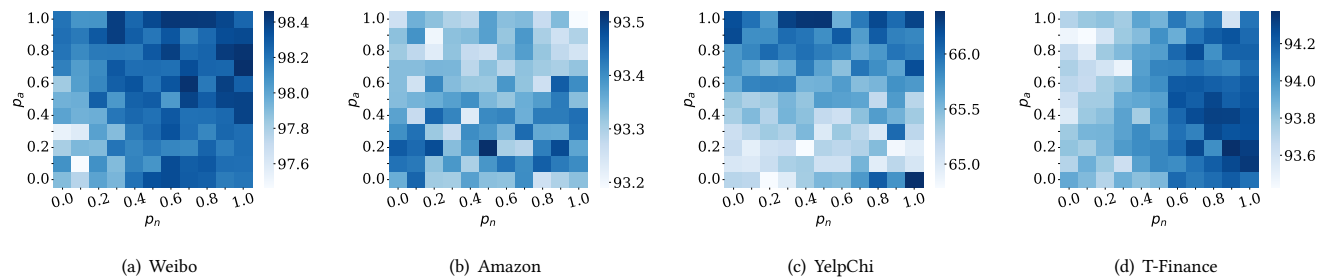


Figure 13: How the AUROC score of GRACE+PAF varies with different values of p_a and p_n .